

Predicting COVID-19 Transmission to Inform the Management of Mass Events: a model-based approach

Claire Donnat, Freddy Bunbury, Jack Kreindler, David Liu, Filippos T. Filippidis, Austen El-Osta, Tonu Esko, Matthew Harris

Submitted to: JMIR Public Health and Surveillance
on: May 24, 2021

Disclaimer: © The authors. All rights reserved. This is a privileged document currently under peer-review/community review. Authors have provided JMIR Publications with an exclusive license to publish this preprint on its website for review purposes only. While the final peer-reviewed paper may be licensed under a CC BY license on publication, at this stage authors and publisher expressly prohibit redistribution of this draft paper other than for review purposes.

Table of Contents

Original Manuscript..... 5

Supplementary Files..... 51

 Figures 52

 Figure 1..... 53

 Figure 2..... 54

 Figure 3..... 55

 Figure 4..... 56

 Multimedia Appendixes 57

 Multimedia Appendix 1..... 58

Predicting COVID-19 Transmission to Inform the Management of Mass Events: a model-based approach

Claire Donnat¹ PhD, MSc, BSc; Freddy Bunbury² PhD, MRES, BA; Jack Kreindler³ MD; David Liu¹; Filippas T. Filippidis³; Austen El-Osta³; Tonu Esko⁴; Matthew Harris³

¹University of Chicago Department of Statistics Chicago US

²Carnegie Institution for Science Department of Plant Biology Stanford US

³Imperial College School of Public Health London GB

⁴University of Tartu Tartu EE

Corresponding Author:

Claire Donnat PhD, MSc, BSc
University of Chicago
Department of Statistics
5747 South Ellis Avenue
Chicago
US

Abstract

Background: Modelling COVID-19 transmission at live events and public gatherings is essential to control the probability of subsequent outbreaks and communicate to participants their personalised risk. Yet, despite the fast-growing body of literature on COVID transmission dynamics, current risk models either neglect contextual information on vaccination rates or disease prevalence or do not attempt to quantitatively model transmission.

Objective: This paper attempts to bridge this gap by providing informative risk metrics for live public events, along with a measure of their uncertainty.

Methods: Building upon existing models, our approach ties together three main components: (a) reliable modelling of the number of infectious cases at the time of the event, (b) evaluation of the efficiency of pre-event screening, and (c) modelling of the event's transmission dynamics and their uncertainty along using Monte Carlo simulations.

Results: We illustrate the application of our pipeline for a concert at the Royal Albert Hall and highlight the risk's dependency on factors such as prevalence, mask wearing, or event duration. We demonstrate how this event held on three different dates (August 20th 2020, January 20th 2021, and March 20th 2021) would likely lead to transmission events that are similar to community transmission rates (0.06 vs 0.07, 2.38 vs 2.39, and 0.67 vs 0.60, respectively). However, differences between event and background transmissions substantially widen in the upper tails of the distribution of number of infections (as denoted by their respective 99th quantiles: 1 vs 1, 19 vs 8, and 6 vs 3 for our three dates), further demonstrating that sole reliance on vaccination and antigen testing to gain entry would likely significantly underestimate the tail risk of the event.

Conclusions: Despite the unknowns surrounding COVID-19 transmission, our estimation pipeline opens the discussion on contextualized risk assessment by combining the best tools at hand to assess the order of magnitude of the risk. Our model can be applied to any future event, and is presented in a user-friendly R Shiny interface.

(JMIR Preprints 24/05/2021:30648)

DOI: <https://doi.org/10.2196/preprints.30648>

Preprint Settings

1) Would you like to publish your submitted manuscript as preprint?

✓ **Please make my preprint PDF available to anyone at any time (recommended).**

Please make my preprint PDF available only to logged-in users; I understand that my title and abstract will remain visible to all users.
Only make the preprint title and abstract visible.

No, I do not wish to publish my submitted manuscript as a preprint.

2) If accepted for publication in a JMIR journal, would you like the PDF to be visible to the public?

✓ **Yes, please make my accepted manuscript PDF available to anyone at any time (Recommended).**

Yes, but please make my accepted manuscript PDF available only to logged-in users; I understand that the title and abstract will remain visible to the public.

Yes, but only make the title and abstract visible (see Important note, above). I understand that if I later pay to participate in <http://www.jmir.org/>, I will be able to make my accepted manuscript PDF available to the public.



Original Manuscript

Predicting COVID-19 Transmission to Inform the Management of Mass Events: a model-based approach

Claire Donnat^{1*}, Freddy Bunbury², David Liu¹, Jack Kreindler^{3,4}, Filippos T. Fillipidis⁴, Austen El-Osta⁴, Tõnu Esko⁵ and Matthew Harris⁴.

Abstract

Background:

Modelling COVID-19 transmission at live events and public gatherings is essential to control the probability of subsequent outbreaks and communicate to participants their personalised risk. Yet, despite the fast-growing body of literature on COVID transmission dynamics, current risk models either neglect contextual information on vaccination rates or disease prevalence or do not attempt to quantitatively model transmission.

Objective:

This paper attempts to bridge this gap by providing informative risk metrics for live public events, along with a measure of their uncertainty.

Methods: Building upon existing models, our approach ties together three main components: (a) reliable modelling of the number of infectious cases at the time of the event, (b) evaluation of the efficiency of pre-event screening, and (c) modelling of the event's transmission dynamics and their uncertainty along using Monte Carlo simulations.

Results: We illustrate the application of our pipeline for a concert at the Royal Albert Hall and highlight the risk's dependency on factors such as prevalence, mask wearing, or event duration. We demonstrate how this event held on three different dates (August 20th 2020, January 20th 2021, and March 20th 2021) would likely lead to transmission events that are similar to community transmission rates (0.06 vs 0.07, 2.38 vs 2.39, and 0.67 vs 0.60, respectively). However, differences between event and background transmissions substantially widen in the upper tails of the distribution of number of infections (as denoted by their respective 99th quantiles: 1 vs 1, 19 vs 8, and 6 vs 3 for our three dates), further demonstrating that sole reliance on vaccination and antigen testing to gain entry would likely significantly underestimate the tail risk of the event.

Conclusions: Despite the unknowns surrounding COVID-19 transmission, our estimation pipeline opens the discussion on contextualized risk assessment by combining the best tools at hand to assess the order of magnitude of the risk. Our model can be applied to any future event and is presented in a user-friendly R Shiny interface [88]. Finally, we discuss our model's limitations, as well as avenues for model evaluation and improvement.

Keywords: COVID-19; Transmission Dynamics; Live Event Management; Monte Carlo Simulation;

Introduction

More than a year after a global, unprecedented cancellation of live events in March 2020, the future

of live events and the entertainment industry remains uncertain despite increasing vaccination rates and low community prevalence levels (at the time of writing). The main concern raised by these gatherings lies in their susceptibility to “super-spreading” — a scenario whereby a few contagious participants inadvertently infect a disproportionately large number of others [1-6], and which has been highlighted as a significant driver of the pandemic [7-11]. Despite the re-opening of live events in the UK on July 19th 2021, the threat of existing and emergent COVID-19 variants coupled to dwindling immunity from vaccination over time suggests that policy makers and event organizers will likely continue to struggle with the following two questions: (a) Is the COVID-19 transmission risk posed by these events tolerable? and (b) What additional safety measures can be feasibly deployed to reduce this risk?

The answer to these questions is inherently tied to the estimation of two quantities: the number of infections occurring at the event, and the post-event secondary attack rate, or number of subsequent infections in the participants’ social circles. Evaluating the safety (or lack thereof) of large public gatherings can then be reframed as quantifying the significance and magnitude of their effect on the distribution of the number of primary and secondary COVID-19 cases. Yet, despite the growing body of literature on COVID-19 risk evaluation and recent efforts to evaluate the safety of live events, this effect remains ill-characterized. Nevertheless, over the past several months, several calculators were developed to estimate this risk [12-15]. These methods can typically be placed in one of three categories.

(a) *Ranking heuristics*: These estimators typically rank events on a scale ranging from “low” to “high” risk based on the feedback of medical experts [13, 16-18]. However, these heuristics do not take into account contextual information, including the prevalence. The risk associated with an event would be classified as high regardless of whether it was held in August 2020 (background prevalence of 1 in 3,000 individuals in the United Kingdom) or January 2021 (prevalence of 1 in 60 individuals [2]).

(b) *Context-based heuristics*: These calculators estimate the probability of encountering one COVID case based on the number of people attending an event [12, 13]. Whilst more context-aware than risk assessment charts, such estimators do not attempt to model transmission dynamics — which is undeniably one of the main unknowns in the spread of viral epidemics — and consequently rarely stratify risk by type of activity. To exemplify, a classical music recital of 1.5 hours for the BBC Proms would potentially be considered equally risky to a 3-hour concert in which participants could be expected to sing along.

(c) *Transmission risk calculators*: Stemming from the physics or fluid dynamics, these calculators focus on modelling the aerosolization and spread of micro-droplets — typically in a closed/indoor environment [19-22]. These fine-grained models thus must be combined with extensive and often prohibitive simulations of crowd movements in order to model transmission dynamics during any given event.

Regardless of their category, most of these models rely on a large number of input parameters, including (but not restricted to) the prevalence of the disease. Whilst certain calculators attempt to bridge the gap between expert heuristics and physical models [12, 23], they are not capable of predicting the risk of a future event. Moreover, all of these estimators provide point estimates – in other words, their output is a single number to quantify the risk. Given the uncertainty associated with all the inputs and the parametrization of the problem as well as the high stochasticity of viral transmission, the provision of a single consolidated outcome or number can potentially be misleading. This is because a singular focus on the expected outcome precludes consideration of the distribution of all possible outcomes, including worst-case scenarios. In the context of COVID-19 where the majority of new cases has been shown to be caused by a minority of index cases [74-76], the modelling of tail events and potential super-spreader phenomena takes on a significant

importance in risk assessment [92-93].

Mitigating transmission risk.

Meanwhile, with the increasing vaccination rates in several countries around the world, a few initiatives have begun to evaluate the outbreak risk associated with live events empirically [24-27]. This is because vaccinated individuals may still be infected with SARS-CoV-2 [28, 29], and even antigen-test based screening of ticket holders offers no guarantee due to false negatives [30, 31]. The estimation of what constitutes an admissible level of risk thus poses a difficult conundrum to the live event industry. To begin answering these questions, the CAPACITY study [32] – a partnership between CERTIFIC (a private, remote testing, health status and identify certification service) and Imperial College London – aims to predict and measure the outcomes of full capacity live events whilst ensuring rigorous implementation and alignment to current public health and recommended safety measures. Central to this study is the provision of a streamlined and efficient pre-event screening protocol of all ticket holders using professionally witnessed rapid at-home antigen tests followed by post-event monitoring based on antigen tests, surveys and safety recommendations (see Appendix D). In this setting, *providing risk estimates not only becomes essential in communicating to the ticket holders their own level of risk so that they may make an informed decision of whether to attend the event, but also necessary to inform event managers and policy makers on the likelihood of an outbreak* – a task which serves here as the motivating application behind this paper.

A working example: Concert at the Royal Albert Hall.

In order to understand and illustrate the potential challenges that arise in the risk estimation for the CAPACITY study, we consider as an example a concert at the Royal Albert Hall (RAH) and demonstrate how to estimate the associated risk assuming a near capacity attendance of 5,000 in the main concert hall, which has a volume of 86,650 m³ [33], with a dwell time of 3 hours. Attendees will be assumed to be a cross-section representative of the general British public and will be required to have a negative COVID antigen test result within 2 days prior to the event, as well as satisfying other self-declared symptoms and exposure-risk questions. Vaccination status would be requested, but not required for attendance, and full compliance with mask wearing is assumed in our default example.

Goals and Contributions.

The objectives of our modelling approach are three-fold: (a) enable the quantitative comparison of different activities and event characteristics, (b) estimate the efficacy of various safety protocols and (c) provide a predictive risk assessment, i.e. the risk associated with a scheduled future event. To this end, we delineate our approach into three sequential steps (see Fig. 1): 1) estimating the number of contagious participants, 2) evaluating the transmission dynamics, and 3) comparing the risk of holding the event with the null model i.e. if the event had not taken place. We illustrate the application of our risk modelling pipeline in the RAH example to highlight the risk's dependency on factors such as prevalence, mask wearing, number of attendees and event duration. In particular, we demonstrate how this particular event held on three different dates corresponding to three distinct COVID prevalence regimes in the UK (stable low prevalence: August 20th 2020; high prevalence peak: January 20th 2021; medium declining prevalence: March 20th 2021) would likely lead to transmission events that are on par with community transmission rates (0.06 vs 0.07, 2.38 vs 2.39, and 0.67 vs 0.60 respectively (see Table 2)). However, the 99th percentile of the prediction interval for the infections at the event would likely be substantially higher than the background rate (1 vs 1, 19 vs 8, and 6 vs 3 respectively), further demonstrating that sole reliance on vaccination and antigen testing to gain entry **would significantly underestimate the tail risk of the event**. However, we emphasize that the goal of this paper is not to present a novel “state-of-the-art” risk estimation

procedure. This is because COVID-19 transmission mechanisms remain poorly characterized, and we acknowledge that our approach requires certain simplifications and assumptions which we discuss at length in the last section of this paper. Rather, faced with the need to provide a risk evaluation tool despite many unknowns, our estimation pipeline combines the best tools at hand to assess the order of magnitude of the risk – thereby opening the avenue for further work on contextualized COVID risk assessment. Consequently, in providing a pipeline for risk-estimation, our objective is two-fold: (i) developing a publicly available platform to increase risk awareness and promote informed consent for event organizers and participants, while simultaneously (ii) encouraging the data collection that is currently so desperately needed for risk assessment. Our model can be applied to any event occurring in the near future and is presented in a user-friendly R Shiny interface [88].

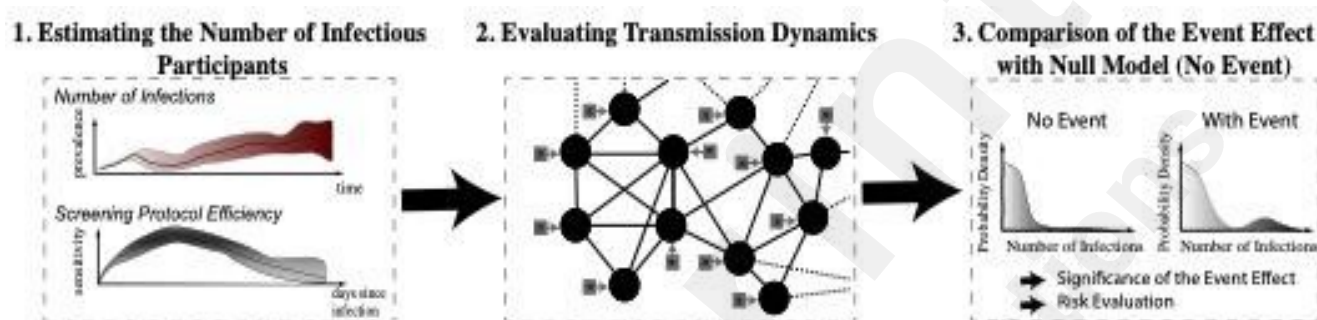


Figure 1. Summary of our modelling pipeline.

Methods: Modelling the Risk of a Large Public Event

Step 1: Estimating the Number of Infectious Participants

Step 1a. Projected Incidence.

The first step in our risk modelling procedure is to predict the number of infectious cases attending a given future event. COVID forecasting is undeniably an involved task, as reflected by its impressive corresponding body of literature (e.g. agent-based models, or Susceptible- Exposed- Infectious- Removed (SEIR) models [34-44]). Predicting the number of new cases per day typically depends on the choice of a specific parameterization (e.g. an exponential growth for computing the reproductive number R [45, 46]), whose validity is severely hindered by continuous updates in public policies. To alleviate these concerns, we use a non-parametric k-nearest neighbour (kNN) approach. Using all trajectories of the disease incidence across countries and time since the beginning of the pandemic, we compute the $k = 100$ closest trajectories (in terms of the l_2 loss) on time windows of two weeks. The historical trajectories of these k-nearest neighbours are then used as a “dictionary of observed behaviours” to predict the daily incidence rate in the days leading to the event. We defer to Appendix A for a more in-depth discussion of this estimation procedure, a description of the parameter selection process, as well as an evaluation of its performance compared to standard epidemics prediction methods. To briefly summarize, our k-NN approach provides a non-parametric, model-agnostic approach to epidemic prediction that is more robust to non-stationarity in public policies than model-based approaches. We show in Appendix A that these parameters ($k=100$ neighbours, fitted on trajectories of 14 days) are optimal in allowing an accurate estimation of the trajectory whilst providing adequate coverage and uncertainty quantification. In fact, we show that while standard methods fail to provide reliable uncertainty estimates, our k-NN methods provides a

coverage greater than 95%. Despite coming at the price of wider prediction intervals, our pipeline privileges methods that allow to correctly estimate the uncertainty in its outputs – thereby more accurately reflecting the state of our knowledge (or lack thereof). Figure 2 presents a comparison of the projected incidence for our three dates of interest (August 20th 2020, January 20th 2021, March 20th 2021) for the RAH concert using two weeks of fitting, and predicting four weeks in advance. Note the good coverage provided by our method (the convex hull of the 95% prediction intervals for the projected incidences contains the actual observations). These plots also highlight the importance and variability of the incidence, which varied by orders of magnitude between August 2020 and January 2021.

Step 1b. Under-ascertainment Bias.

The estimated number of new cases based on official incidence data will then need to be corrected for under-ascertainment. The latter refers to the downward bias of the reported prevalence in the population, due for instance to limited testing capacity, low test sensitivity or people being unwilling or unable to take a test. To this end, we compare the ratio of the number of deaths over reported cases (translated by three weeks) to an expected, age-stratified Infection- Fatality Ratio [4] (see Appendix A for more details). To highlight the potential importance of this correction step, the ascertainment rate for the United Kingdom was evaluated as over 90% for August 2020, but below 40% for December 2020.

Step 1c. Determining the Number of Infectious participants at the event.

Having predicted the background daily incidence rate, we turn to the estimation of the number of infectious participants who will attend the event despite the screening protocols. For an infectious individual to attend the event in spite of the CAPACITY study's screening protocol, they must (a) have no COVID-like symptoms or fail to report them on the morning of the event, (b) receive a (false) negative result during antigen testing $D = 2$ days prior to the event, and (c) be contagious (rather than simply infected) at the time of the event. We evaluate the joint probability of these events as follows, and, for the sake of clarity, refer the reader to Appendix A for an in-depth explanation of our estimation procedure.

(a) Symptoms-Check Failure. One of the main challenges associated with the COVID- 19 crisis is the number of asymptomatic cases - that is, infected individuals that do not express symptoms and are thus unaware of their potential infectiousness. This group includes individuals that are either pre-symptomatic or completely asymptomatic during the course of their illness – the latter are estimated to represent roughly 25% of all cases [47]. For symptomatic patients, the probability of having symptoms on the day of the event is also a function of time since infection. To account for this temporal dependency, we use estimates of the incubation period (defined as the number of days between infection and symptom onset) from McAloon et al. [48] and data on symptoms duration from van Kampen et al. [49] to estimate the probability for a ticket holder infected k days before the event to exhibit symptoms on the day of the event. A density plot of this probability is displayed in red in Figure 3a.

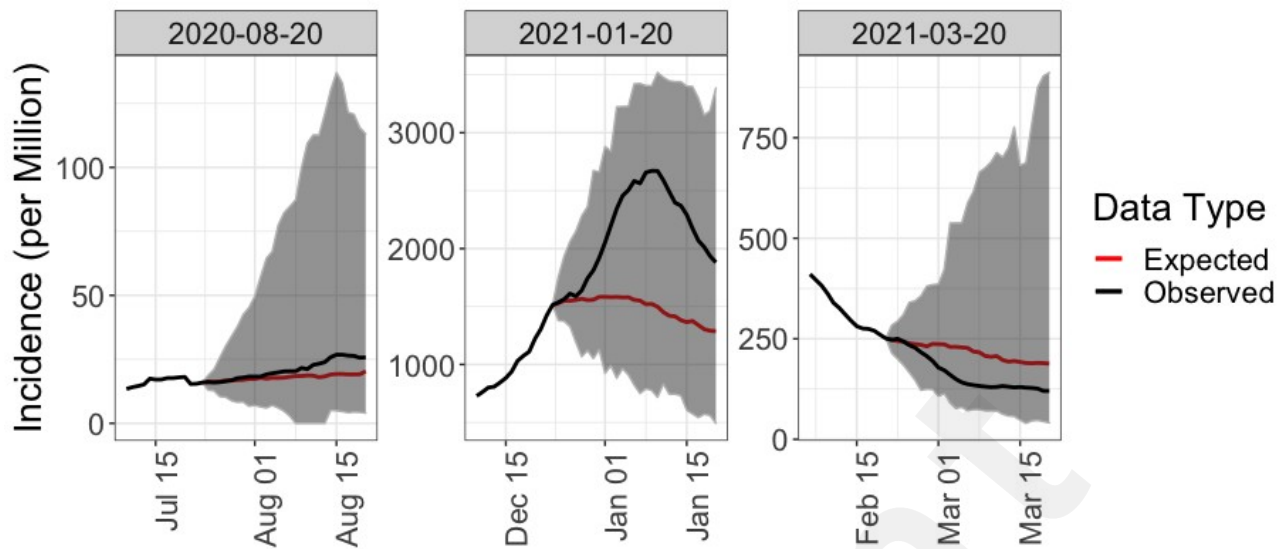


Figure 2: Projected incidence (average and 95% prediction interval) using a 100-nearest neighbour approach. The black line denotes observed incidence rates, while the red denotes the predicted ones (based on initial period of observation of $d=14$ days). The prediction interval for the predicted incidence over the next four weeks is highlighted in dark grey. We note that our k-NN method provides good coverage (the observed trajectory lies within the 95% prediction interval).

(b) *Antigen test failure.* The sensitivity of COVID tests depends heavily on the time since infection — whether these are the gold-standard PCR or Lateral Flow Antigen Assays [50]. Moreover, studies have shown that LFA tests have much lower sensitivity on asymptomatic individuals than symptomatic: in particular, according to a recent CDC report [51], Rapid Antigen testing has 80% sensitivity on symptomatic individuals, but only 40% sensitivity on asymptomatic individuals. Coupling the sensitivity estimates [50, 51] with the distribution of incubation period and estimated percentage of asymptomatic cases [48, 47], for each individual infected at day k taking an antigen test D days before the event, the probability of getting through the filtering protocol is thus given by the formula:

$$p = P[\text{Contaminated at time } k] = (1 - s_{t-k-D}^{(\text{symptomatic})}) (p_{SC} \times p_{t-k}^{(\text{symptom})} + (1 - p_{t-k}^{(\text{symptom})})) + p^{(\text{asymptomatic})} (1 - s_{\square}^{(\text{asymptomatic})})$$

where $s_{t-k-D}^{(\text{symptomatic})}$ and $s_{\square}^{(\text{asymptomatic})}$ are respectively the sensitivities of the test taken D days before the event for a symptomatic participant infected $t-k$ days before the event and an asymptomatic individual. The parameter $p_{t-k}^{(\text{symptom})}$ denotes the probability for a symptomatic individual to exhibit symptoms $t-k$ days after infection, whereas $p^{(\text{asymptomatic})}$ is the probability of being asymptomatic. Finally, the variable p_{SC} denotes the probability of the Symptoms Check failing — namely, that the participant does not want to report their symptoms (see Appendix A for more details). The curve in black on Figure 3b shows the probability of the failure of the screening protocol as a function of days after infection. The shaded areas denote the uncertainty around this estimate due to the variability of the incubation time.

(c) *Infectiousness.* The infectiousness of the participants — that is, the propensity of an infected ticket holder to contaminate others — is a function of time since infection. In order to estimate this relationship, we build upon the existing literature studying the link between RT-PCR thresholds and cultivable virus [52, 53]. The percentage of culturable viral material in the sample can indeed be used as a proxy for infectiousness. Using the estimated percentages of viable samples [52, 53] as a function of time since symptom onset, compounded with distribution of the incubation period duration [48], we compute an estimate of the infectiousness as a function of time since infection (black curve in Figure 3a). A more complete description of this estimation procedure is presented in

Appendix A. The results are presented in Figure 3b. The red line in Figure 3b shows the resulting probability for an infectious ticket holder to pass through the screening protocol and be allowed into the event. Note that ticket holders that have been infected five days before the event are the most likely to be infectious and let in the venue on the day of the event.

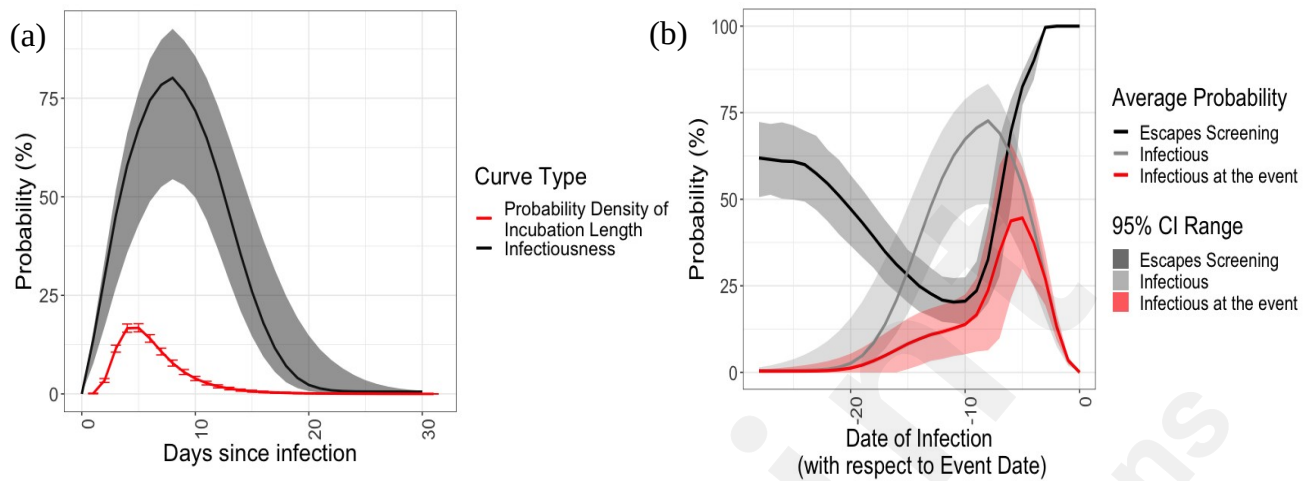


Figure 3: (a) Density of the COVID-19 incubation time, and Percentage culture positive. (b) Probability that an individual is infectious (light grey), that the screening protocol will miss them (black), and that they will be missed and so attend the event (red), as a function of days since infection. The shaded regions denote the uncertainty of this estimate due to the uncertainty on the sensitivity of the test. The distribution of the incubation time already integrates the uncertainty on the parameters μ and σ of the log-normal distribution.

Step 1d. Determining the number of participants at risk.

Finally, the last quantity that we need to infer before getting into the specifics of the transmission mechanisms is the number of participants at risk of being infected who present at the event. This requires a knowledge of the participants' COVID susceptibility status, i.e., has the participant already had COVID in the previous year and/or has the participant been vaccinated? While previous history could be imputed through additional questions (e.g., previous positive test for COVID, symptoms, etc, combined in a model such as in [54]), for the sake of simplicity, we only consider the vaccination status of the participants — thus leaving out the proportion of the population that had COVID but was not yet vaccinated. This induces a risk estimate that is biased upward and is thus more conservative. We impute missing data (cases where the participants have not filled in their vaccination status) using linear regression, expressing vaccination rate as a function of time. This assumes that vaccinations are operating at capacity (see Appendix A for a longer discussion on the reasons for this approximation, and further ways of improving this model). Having imputed the rate of new vaccinations $\pi_s, s=1 \dots t$ in the days leading to the event, we turn to the estimation of the number of individuals that are likely to be susceptible. Recent reports indicate that vaccine-acquired immunity is a function of both time since vaccination and number of doses [55]. To compute the effective number of participants at risk in the event, we use a compound Poisson distribution: on each day s in the weeks leading to the event, the number X of new participants vaccinated (having either their first or second dose) is expressed as a Poisson $(\pi^{(dose j)})$, where $j \in \{1, 2\}$. Each of these newly vaccinated individuals then has a probability $\rho^{(dose j)}$ of being immune, depending on the date and dose j that they have received. The resulting number of immune people Z attending the event can thus be modelled as:

$$Z \sim \text{Poisson} \left(\sum_{j=1}^2 \square \sum_{s=1}^T \square \pi_s^{(dose j)} \rho_{t-s}^{(dose j)} \right).$$

We discuss in Appendix A how this estimation can easily be modified as the vaccination rates

increase and the Poisson approximation becomes no longer valid.

Royal Albert Hall Example.

For the RAH example, we present a comparison of each quantity for three different dates (see Table 1). Of note is that the screening safety protocol is effective in more than 60% of cases that when combined with the expected infectiousness of participants and self-reporting of COVID-like symptoms, imply that 95% of infected cases are removed. We also note that prevalence is very important in determining the number of infectious cases at the event — thereby highlighting the importance of a context-aware risk calculator.

| Date of the Event | August 20 th 2020 | January 20 th 2021 | March 20 th 2021 |
|--|------------------------------|-------------------------------|-----------------------------|
| Projected incidence | 20 in 1,000,000 | 1,286 in 1,000,000 | 188 in 1,000,000 |
| Number of Infected Participants | 3.6 | 299.3 | 50.2 |
| Number of Infectious Participants at the Event | 0.22 | 7.96 | 2.00 |
| Percentage of Caught Cases | 94% | 97% | 96% |
| Number of Susceptible Participants | 4,996.4 | 4700.7 | 3860.4 |

Table 1: Comparison of the efficiency of the screening protocol and the number of infectious participants at the event by date. The combined effect of the screening protocol, and the natural time-dependent infectiousness of infected ticket holders mean that the number of infectious participants at the event is likely to be very low (~ of the order of tens in times of extremely high prevalence). Note that on March 20th, vaccinations rates were starting to account for a substantial proportion of the British public, so that the sum of the number of susceptible participants with the number of infected participants does not equate 5,000.

Step 2: Modelling Transmission Dynamics

Having estimated the number of infectious participants at the event, the second major component of our model consists of estimating the number of transmission events during the event itself.

Identification of transmission mechanisms.

More than a year after the start of the epidemic, the precise mechanisms by which COVID-19 is transmitted are still unclear. Aside from direct physical contact, experts continue to debate the significance of the following two main routes of infection:

(a) *Droplet transmission.* In this scenario, transmission happens through the inhalation of droplets (particles of 5 to 10 μm in diameter [56]), and typically occurs when a person is in close proximity (within 1 meter) with someone who has respiratory symptoms (e.g., coughing or sneezing).

(b) *Airborne transmission.* Increasing concerns around airborne transmission have been raised by a number of experts over the past few months [57, 58]. Airborne transmission refers to the presence of the virus within droplet nuclei remaining in the air for long periods of time and with the potential to travel long distances [57] and penetrate more deeply in respiratory tracts. Airborne transmission has been estimated to be nearly 19 times more likely indoors than outdoors [59]. In the context of large public events, this transmission route thus has more diffusive power and hence could explain several super-spreader events (SSEs) [6] making it a major cause for concern [53, 2, 57, 60-66].

While droplet emission is undeniably a source of concern and a major source of transmission, simple safety precautions such as mask wearing have been shown to efficiently control this transmission source [67, 68]: it is estimated that face masks can block 80% of exhaled droplets and reduce inhaled

droplets by up to 50%, and so on average reduce the transmission probability by 70% [67]. Conversely, the evidence concerning the efficiency of standard protective equipment in filtering aerosol droplets varies widely across studies probably due to “variation in experimental design and particle sizes analysed” [67]. Airborne transmission in indoor settings can thus represent one of the main risk factors in live events, which we focus on modelling using the aerosol model proposed by Jimenez [69, 63]. The Jimenez aerosol transmission model [69, 21, 63, 70] is currently one of the only COVID-transmission models that provides enough granularity to quantify the risk associated with an event. This recognized model has been used several times in the literature over the course of the pandemic, including to allow in-class teaching at the University of Illinois at Chicago [64]. Based on the Wells-Riley model [71-73], this estimator calibrates the quanta to known transmission events, and considers important factors to compute a risk estimate, including event-specific (number of people, local prevalence, etc) and venue-specific variables (ventilation rate, size of the venue, UV exposure). This Wells-Riley-based model relies on the evaluation of three quantities: (a) *the quanta exhalation rate*, which is contingent on the activity performed and the number of infectious participants; (b) *quanta concentration*, which is a function of the volume of the space, the room ventilation rate, and the quanta exhalation rate; and (c) *quanta inhalation rate*, which is a function of the quanta concentration and breathing rate associated with the activity performed. The probability for each susceptible individual to be infected can then be written as: $p_{infection} = 1 - e^{-q_{inhalation}}$. See Appendix B for more details).

Modelling the uncertainty of the model.

To estimate the uncertainty associated with this model, we use Monte-Carlo simulations. We simulate random input parameters (number of infectious and susceptible individuals) using the distributions and uncertainty estimates discussed in the previous section. In order to model the uncertainty associated with the aerosol transmission model, we add a sampling step at the end of the Jimenez pipeline. This allows us to account for individual variations in infectious participants’ ability to spread the disease, and to remain consistent with the extensive literature on the heavy-tailed Pareto nature of COVID transmission and superspreading [74-76]. For each infected participant, we sample the number of quanta that they exhale using a Pareto distribution with shape $\theta = 1.16$ and rate $\eta = \theta / (\theta - 1) q^{\text{exhalation}}$. This produces a distribution centred around $q^{\text{exhalation}}$ but skewed to the right and heavy-tailed – thereby modelling the heterogeneity in infected participants’ ability to spread. This choice of parameters allows us to abide by the Pareto principle, according to which 80% of transmissions are due to 20% of those infected. In accordance with the uniform mixing assumption of the aerosol transmission models, susceptible participants then all inhale a quanta concentration that is a function of the sum of the exhaled quanta: all have an identical probability of becoming infected. In mathematical terms, infections are thus simulated using a binomial distribution such that: $n_{infected} \sim \text{Binomial}(n_{susceptible}, 1 - e^{-q_{inhalation}})$. We discuss the limitations of this approach and its assumptions in the discussion section of this paper.

Results

Step 3: Comparison with the Null Model

To quantify the effect of the event, it is necessary to put it in context of the background rate of infections: even if the participants had not been to the event, they could have been infected elsewhere. In this null model, the number of infections is binomially distributed, such that the number infections Y is $Y \sim \text{Binom}(n_{susceptible}, \pi)$.

The Royal Albert Hall. We present the results for the RAH example in Table 2. This table shows in

grey the values of the different quantiles of this distribution. We note the skewed distribution that we obtain is expected given the modelling of the uncertainty around inhalation rate. If the event did not occur, then on each respective date there would be an expected community transmission of 0.07 (95% prediction interval: 0, 1), 2.5 (0, 7) and 0.63 (0, 3) events on August 20th 2020, January 20th 2021 and March 20th 2021, respectively. However, with the event taking place on these dates, and calculating the expected number of infectious individuals, susceptible individuals and transmission dynamics within the venue, the distribution of the number of transmission events would in general widen to 0.06 (0, 1), 2.38 (0, 19) and 0.67 (0, 6) in that same order. In this case, it is important to note the similarity in mean transmission between the “event” and “no event” scenarios, and their substantial deviation in the tails. This highlights the importance of modelling the distribution of the risk, and highlighting its substantial heavy tails, rather than providing point estimates.

It is likely, although not inevitable, that the event will have an impact on the transmission and increase it irrespective of the level of the prevalence. However, for low levels of prevalence and higher vaccination rates, this substantially decreases. Having computed the number of expected transmission events, we can then compute several complementary metrics of interest including for example the secondary attack rate (SAR) — that is, the number of COVID cases in the participants’ community in both the null and the event model. SAR can be calculated from the predicted reproductive rate (R) in the regions where the ticket holders dwell. In the UK, R rates are updated on a weekly basis at regional levels (e.g. East Midlands, London etc) and available from the Office for National Statistics, or can be derived from the kNN modelling previously described. An opportunity for further research would be to estimate SAR within households by gathering contextual data from ticket holders. Equally, estimates of hospitalizations and deaths might be possible based on individual characteristics and comorbidities, however this is beyond the scope of the current article.

Evaluating the Effectiveness of the Screening Protocol.

This risk modelling pipeline also allows comparison of different protocols and situations. For example, this pipeline highlights (a) the importance of event duration: the longer the dwell time at the event, the more at-risk the participants, and (b) the importance of wearing masks. Table 3 quantifies outcomes of holding the event on our three dates, assuming that either 0, 50 or 100% of participants are wearing masks, or varying parameters such as the density or length of the concert. Figure 4 completes that analysis by providing a visual representation the effect of these parameters on the distribution of the number of infections.

| Date of the Event | August 20 th , 2020 | | January 20 th , 2021 | | March 20 th , 2021 | |
|-------------------|--------------------------------|------|---------------------------------|------|-------------------------------|------|
| | Event | Null | Event | Null | Event | Null |
| Median | 0 | 0 | 1 | 2 | 0 | 0 |
| Mean | 0.06 | 0.07 | 2.38 | 2.49 | 0.67 | 0.63 |
| 1st Percentile | 0 | 0 | 0 | 0 | 0 | 0 |
| 2.5th Percentile | 0 | 0 | 0 | 0 | 0 | 0 |
| 97.5th Percentile | 1 | 1 | 10 | 7 | 3 | 3 |
| 99th Percentile | 1 | 1 | 19 | 8 | 6 | 3 |

Table 2: Quantiles of the number of transmission events for the RAH concert. We have assumed that all participants were wearing masks, so that the exhalation of particles is reduced by 70%, and

inhalation by 50%.

| Event | 2020-08-20 | 2021-01-20 | 2021-03-20 |
|------------------------------|----------------|---------------|---------------|
| No mask 3h N=5,000 | 0 / 0.3 (0, 4) | 5/9.9 (0, 76) | 1/ 2.4 (0,21) |
| 50 % mask 3h N=5,000 | 0/0.2 (0, 3) | 3/5.5 (0, 40) | 1/1.3 (0, 13) |
| 100% mask 3h N=5,000 | 0/0.1 (0, 1) | 1/2.4 (0, 19) | 0/0.7 (0, 6) |
| 100% mask 1.5h N=5,000 | 0/0.04 (0, 1) | 0/1.4 (0,10) | 0/0.4(0, 3) |
| 100% mask 3h N=2,500 | 0/0.2 (0, 1) | 0/0.9 (0,8) | 0/0.2 (0, 3) |

Table 3: Effect of different input parameters on the quantiles of the number of infections for an event at the RAH across all three dates (Median/Mean (99% Confidence Interval)). Where variables are not mentioned, the number of attendees is 5,000, the duration is 3 hours, and the proportion of attendees wearing masks is 100%.

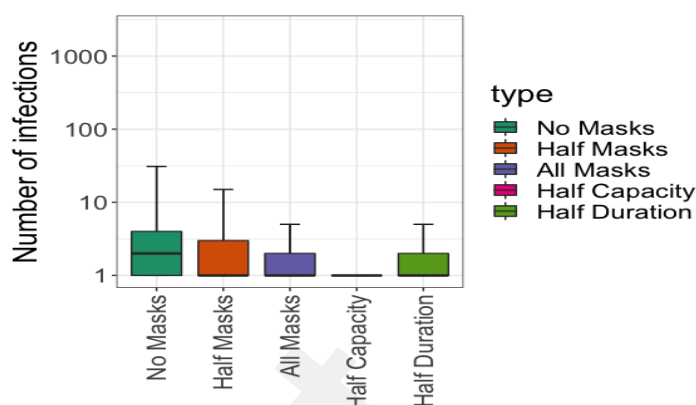


Figure 7: Boxplots showing the distribution of the number of infections across different scenarios, for our RAH event held on March 20th 2021. Where variables are not mentioned, the number of attendees is 5,000, the duration is 3 hours, and the proportion of attendees wearing masks is 100%. Note that the distributional nature of these results is essential in highlighting nuances between scenarios: while holding an event at half capacity, or for half the duration produces average transmission risk that are roughly similar, holding the event at half capacity seems to more substantially reduce the effect of the event in the tails of the distribution.

In addition to the aggregated risk that a live event presents, individual risk of transmission can be estimated and can be communicated to ticket holders so that they can gauge whether the risk of attending the event outweighs their desire to attend. For the first person to purchase a ticket, risk of transmission will be calculated based on their own immunity status (vaccination, regional prevalence etc) and a synthetic population based on national prevalence at that time. As more bookings are assigned to ticket holders, the reliance on the synthetic population decreases as understanding of the number of susceptible and potentially infectious individuals attending the event increases. Therefore, the confidence in the risk score increases as the event draws closer and as the proportion of tickets sold increases. This can be reflected in the updated risk scores provided to ticket holders as the event approaches. The individual risk scores can be modified based on alternative scenarios imputed into the risk algorithm. For example, for an individual not yet vaccinated, their risk could be also presented as if they had been vaccinated, offering an opportunity for the individual to appreciate how vaccination could have modified their risk. Such an approach could form the basis for behaviour change interventional studies for promoting health literacy and tackling vaccine hesitancy (see Appendix D). By working in partnership with the live events organizer, individuals that chose to opt out can be reimbursed without delay and the ticket re-sold.

Discussion

The modelling we propose is based on prevalence estimates and screening protocols to calculate the number of infectious and susceptible individuals attending the event as well as transmission dynamics at the venue to predict the number of new infections. Our paper demonstrates the value of estimating attack rates from live events so that they can be appropriately managed. We also demonstrate how individual ticket holders can receive personalized risk scores for contracting COVID-19 at the event which would, for the first time, enable genuine informed consent to be obtained. Although this methodology provides clear benefit to event organizers, local public health

authorities and individual ticket holders, our approach is based on several assumptions which group in two categories: modelling assumptions and parameter sensitivity.

Modelling Assumptions.

As they combine data and tools from different sources, the computations in our pipeline rely on assumptions at three main levels:

(a) *Predicting COVID-19 prevalence.* To predict future COVID-19 incidence, we chose a k-NN approach as it yields a more robust prediction and better uncertainty quantification than most existing parametric methods. One of the downsides of this approach is that it might not generalize very well to entirely novel behaviours or viral variants – in which case well-parameterized methods may outperform our approach as knowledge of transmission, vaccination and other relevant model parameters continues to improve. While prevalence predictions are important for event planners and attendees alike, on the day of the event the more important metric is whether official case rates reflect actual cases, i.e. the ascertainment rate. Historically, this rate has been low due to limited testing facilities, and our method to determine ascertainment using cases, deaths and infection-fatality rates reflects this, but also indicates that ascertainment may exceed 100% in times of widespread testing and low prevalence. It was beyond the scope of this paper to further investigate ascertainment but we expect that future research will clarify the impact of different test types, their false negative and positive rates, and their frequency of use in determining the ascertainment rate.

(b) *Assessing the efficiency of the screening protocol.* Our modelling framework assumes that events will screen participants with COVID-19 tests, such as virtually-witnessed lateral flow antigen tests. Assessing the efficiency of this screening step requires the estimation of (a) the sensitivity of the test, (b) the probability of having symptoms, and (c) the probability of being infectious – all of these quantities being a function of days since infection. Our estimation of each of these quantities is based on published data - with the exception of the probability of Symptom Check failure (i.e., the probability that a participant lies about their symptoms to get in). By default, we select this probability to be 50%, a choice that will be improved upon as the CAPACITY and other similar studies gather behavioural data. However, as shown in Appendix C, this factor has a relatively minor impact on the outcome of the model compared to the uncertainty of the other inputs. Of potentially greater concern is our assumption that the probability of testing negative 2 days before the event is independent (conditionally on time since infection) of a participant's infectiousness during the event. A potential avenue for improvement could consist of determining both test sensitivity and infectiousness as a function of viral load, and estimating the joint probability of the viral load 2 days apart. However, the data required for this approach is – to the best of our knowledge – still lacking and given the variability of the viral load or PCR Ct behaviour, this conditional independence assumption seemed a reasonable first-order approximation.

(c) *Transmission at the event.* The airborne transmission model that we use relies on a homogeneous (well mixed) air hypothesis for an indoor environment. While several other models have been proposed (either breaking the room into compartments or using a distance index) to counter this hypothesis, we highlight (following the discussion by Jimenez [69]) that this is a first order approximation: some participants will have more risk and others less, so that at low quanta concentration, this effect will be averaged out. At very high concentration, the model will likely under-estimate the number of infections, but given the efficiency of the screening protocol and density limitations, we do not expect this scenario to be common. Moreover, while this model was originally developed for indoor transmission, its application to an outdoor setting – where the ventilation rate can be considered infinite, and transmission is more likely to occur through droplets rather than aerosolized particles – can nonetheless provide a conservative estimate of the risk. We are

however currently working on developing a better model for outdoor transmission, relying on a modelling of droplet transmission in crowd bottlenecks. We leave the detail of this separate transmission model to future work. Finally, we note that our model is not tied down to any specific transmission mechanism, and as our knowledge of COVID transmission improves, we can refine and supplant the transmission dynamics with a superior alternative or another model that is deemed more suitable.

Parameter Sensitivity.

While we try to limit the number of input parameters in our pipeline, the sensitivity of the estimates to these inputs (namely, the mask efficiency and population of interest) has to be studied. We refer the reader to Appendix C for a quantitative sensitivity analysis and highlight our conclusions here. In terms of the model parameters, the greatest unknown consists in determining the efficiency of masks and protective equipment - the latter having been shown to vary depending on the mask type and activity. However, we hope to make use of the growing body of literature on the topic to update and refine this important factor. Secondly, our prediction framework assumes that participants at the event have the same probability of infection and vaccination as their regional average. However, this might not be the case as participation in the event may be an incentive to get vaccinated, or conversely might select for less cautious sub-populations. The importance of this sampling frame assumption nonetheless decreases as participants' vaccination status and behavioural data from the CAPACITY study will result in more precise estimates.

Model Validation.

Finally, one of the main current hurdles for developing risk estimators lies in the absence of quality data to validate and benchmark different transmission models – thereby making the task of validating our transmission pipeline a rather daunting task. Indeed, while we can (and have, see Appendix A) check the accuracy of the vaccination and prevalence estimation step, the validation of the transmission model itself is inherently difficult: there are no, or very few available datasets on COVID spread following live events or rigorous accounts of super spreader events, nor are there any statistics on how likely super spreader events are. As such, the majority of super spreader events that are documented currently (a) are generally not detailed enough to untangle the huge variability in context (outdoors vs indoors, activity performed, background prevalence, etc), and (b) suffer from selection bias --- and might not be reflective of the general distribution of live events. To make up for the current lack of testing data, we resort here to the following three strategies:

- **Model checking:** we begin by validating the behaviour of our model estimates on documented Super spreader Events (SSEs) [91] – that is, we confirm that the model outputs (i) present similar tail behaviour as these documented SSEs, and (ii) are predicted as outlier SSE events by our model.
- **Model Validation on (scarce) existing data:** we also consider two documented live indoor concert events [90-91] and use the event parameters as well as the documented transmission statistics to verify that these numbers fall within the realm of feasible outcomes.
- **Prospective Data Gathering:** finally, to overcome the lack of available data, we propose using the R-shiny app as a data collection platform, and encourage users (event organisers, and participants alike) who use the app to record their event in our dataset by filling in a survey [94]. This paves the way for a larger-scale and more detailed record of transmission events at large gatherings, as well as a more precise modelling of transmission dynamics.

This validation and model-assessment step is further described in Appendix E.

Conclusion

A nuanced, data-driven system is required to assess risk at each event informed by the characteristics of all ticket holders and the background risk of transmission concurrent to the event, so that proportionate and specific action can be taken by event organizers and public health authorities. We have detailed our attempt to create such a system and have outlined its predictions and limitations. Our end-to-end risk model is provided in the form of an R-shiny interface. At times of high prevalence, this type of system will ensure events likely to increase transmission can be halted. At times of low prevalence this will ensure events can potentially continue to operate. Learning to live with SARS-CoV-2 will be about implementing systems that support hyper-local, data driven decisions so that far-reaching and highly damaging sector-specific lockdowns can be avoided as much as possible.

Funding

The work of TE has been supported by the Estonian Research Council Grant PRG1291. MH and AEL are supported in part by the NW London NIHR Applied Research Collaboration. Imperial College London is grateful for support from the NW London NIHR Applied Research Collaboration and the Imperial NIHR Biomedical Research Centre. JK is currently Director of Health Optimisation at the Center for Health and Human Performance (London, UK), as well the co-founder and Medical Director of CERTIFIC.

Availability of data and materials

All the data used in this article is referenced throughout the text. The code for the model can be found online on the authors' Github [89], and the results are displayed as a Rshiny app [88].

Competing interests

JK is the medical director and co-founder of CERTIFIC. The authors. C.D, F.B, D.L., A.E.O, M,H, T.E and F.F declare that they have no competing interests.

Author details

¹Department of Statistics, University of Chicago, Chicago, USA. ²Department of Plant Biology, Carnegie Institution for Science, Stanford, USA. ³School of Public Health, Imperial College, London, UK. ⁴, CERTIFIC, London, UK. ⁵Institute of Genomics, University of Tartu, Tartu, Estonia.

*Corresponding author: Claire Donnat

cdonnat@uchicago.edu
Department of Statistics
5747 South Ellis Avenue
Chicago, IL 6063

References

1. Lin J, Yan K, Zhang J, Cai T, Zheng J. A super-spreader of COVID-19 in Ningbo city in China. *Journal of Infection and Public Health*. 2020; 13(7):935-937. doi: [10.1016/j.jiph.2020.05.023](https://doi.org/10.1016/j.jiph.2020.05.023)
2. Majra D, Benson J, Pitts J, Stebbing J. Sars-cov-2 (COVID-19) superspreader events. *Journal of Infection*. 2021; 82(1):36-40. doi: [10.1016/j.jinf.2020.11.021](https://doi.org/10.1016/j.jinf.2020.11.021)

3. Nadal M, Lassel L, Denis M, et al. Role of super-spreader phenomenon in a COVID-19 cluster among healthcare workers in a primary care hospital. *The Journal of Infection*. 2021; 82(5):e13-e15. doi: 10.1016/j.jinf.2021.02.009.
4. Charlotte N. High rate of SARS-CoV-2 transmission due to choir practice in France at the beginning of the COVID-19 pandemic. *Journal of Voice*. 2020; S0892-1997(20)30452-5. doi: 10.1016/j.jvoice.2020.11.029.
5. Atrubin D, Wiese M, Bohinc B. An outbreak of COVID-19 associated with a recreational hockey game—Florida. *Morbidity and Mortality Weekly Report*. 2020; 69(41):1492-1493. doi: 10.15585/mmwr.mm6941a4.
6. Hamner L. High SARS-CoV-2 attack rate following exposure at a choir practice—Skagit county, Washington, March 2020. *Morbidity and Mortality Weekly Report*. 2020; 69(19):606-610. doi: 10.15585/mmwr.mm6919e6.
7. Lewis D. Superspreading drives the COVID pandemic-and could help to tame it. *Nature*. 2021; 590(7847):544-546. doi: 10.1038/d41586-021-00460-x.
8. Gómez-Carballa A, Bello X, Pardo-Seco J, Martínón-Torres F, Salas A. Mapping genome variation of SARS-CoV-2 worldwide highlights the impact of COVID-19 super-spreaders. *Genome Research*. 2020; 30(10):1434-1448. doi: 10.1101/gr.266221.120
9. Zhang Y, Li Y, Wang L, Li M, Zhou X. Evaluating transmission heterogeneity and super-spreading event of COVID-19 in a metropolis of China. *International journal of environmental research and public health*. 2020; 17(10):3705. doi: 10.3390/ijerph17103705
10. Kochanczyk M, Grabowski F, Lipniacki T. Super-spreading events initiated the exponential growth phase of COVID-19 with 0 higher than initially estimated. *Royal Society Open Science*. 2020; 7(9):200786. doi: 10.1098/rsos.200786.
11. Georgia Tech. COVID-19 event risk assessment planning tool. Available from <https://covid19risk.biosci.gatech.edu/>.
12. Mathematica. COVID-19 event risk assessment planning tool, 2020. Available from <https://19andme.covid19.mathematica.org/>.
13. ABC News. What's your risk? Available from <https://abc7news.com/feature/salons-to-dinner-parties-experts-rate-the-risk-of-12-activities/6254129/>.
14. Brown University. My COVID risk. Available from <https://digitalhealth.med.brown.edu/news/2021-05-31/mycovidrisk/>.
15. Illinois State Medical Society. Physician survey of COVID-19 risk for daily activities. 2020. https://www.isms.org/News_and_Publications/Newsroom/News_Releases/Illinois_Physician_Survey_Rates_COVID-19_Risk_for_Daily_Activities/
16. Texas Medical Association. Risk assessment chart. 2020. https://www.texmed.org/uploadedFiles/Current/2016_Public_Health/Infectious_Diseases/309193%20Risk%20Assessment%20Chart%20V2_FINAL.pdf
17. Texas Medical Association. Winter risk assessment chart. 2020. https://www.texmed.org/uploadedFiles/Current/2016_Public_Health/Infectious_Diseases/309640_Winter_Risk_Assessment_Chart_COLOR.pdf
18. Lelieveld J, Helleis F, Borrmann S, et al. Model calculations of aerosol transmission and infection risk of COVID-19 in indoor environments. *International Journal of Environmental Research and Public Health*. 2020; 17(21):8114. doi: 10.3390/ijerph17218114.
19. Mittal R, Meneveau C, Wu W. A mathematical framework for estimating risk of airborne transmission of COVID-19 with application to face mask use and social distancing. *Physics of Fluids*. 2020; 32(10):101903. doi: 10.1063/5.0025476.
20. Peng Z and Jimenez JL. Exhaled CO2 as COVID-19 infection risk proxy for different indoor environments and activities. *Environmental Science and Technology Letters*. 2021; 8(5):392-397. doi: 10.1021/acs.estlett.1c00183
21. Wilson N, Corbett S, Tovey E. Airborne transmission of COVID-19. *BMJ*. 2020; 370:m3206. doi: 10.1136/bmj.m3206
22. The microCOVID Project. Risk tracker. Available from <https://www.microcovid.org/tracker>.
23. Grenier E. Could Germany's COVID concert experiment help arenas hold large events again? *Deutsche Welle*. August 23, 2020. <https://www.dw.com/en/could-germanys-covid-concert->

- experiment-help-arenas-hold-large-events-again/a-54661902/.
24. Schulten L. Dutch researchers test ways to party during the pandemic. Deutsche Welle. March 22, 2021. <https://www.dw.com/en/dutch-researchers-test-ways-to-party-during-the-pandemic/a-56953021/>.
 25. COVID: Barcelona hosts large gig after testing crowd. British Broadcasting Corporation. March 28, 2021. <https://www.bbc.com/news/world-europe-56556451/>.
 26. Moritz S, Gottschick C, Horn J, et al. The risk of indoor sports and culture events for the transmission of COVID-19 (restart-19). medRxiv. Preprint posted November 3, 2020. doi: 10.1101/2020.10.28.20221580.
 27. Centers for Disease Control and Prevention. What you should know about the possibility of COVID-19 illness after vaccination. 2021. <https://www.cdc.gov/coronavirus/2019-ncov/vaccines/effectiveness/why-measure-effectiveness/breakthrough-cases.html/>.
 28. Tinker B, Fox M. So far, 5,800 fully vaccinated people have caught COVID anyway in us, CDC says. CNN. April 15, 2021. <https://www.cnn.com/2021/04/14/health/breakthrough-infections-covid-vaccines-cdc/index.html> [accessed May 1, 2021].
 29. Deeks J, Raffle A, Gill M. COVID-19: government must urgently rethink lateral flow test roll out. BMJ Opinion. January 11, 2021. <https://www.bmj.com/company/newsroom/uk-government-must-urgently-rethink-lateral-flow-test-roll-out-warn-experts/>.
 30. Halliday J. Rapid COVID testing in England may be scaled back over false positives. The Guardian. April 15, 2021. <https://www.theguardian.com/world/2021/apr/15/rapid-covid-testing-in-england-may-be-scaled-back-over-false-positives/> [accessed May 1, 2021].
 31. Harris M, Kreindler J, El-Osta A, Esko, T, Majeed F. Safe management of full-capacity live/mass events in COVID-19 will require mathematical, epidemiological and economic modelling. Journal of the Royal Society of Medicine. 2021; 114(6):290-294. doi: 10.1177/01410768211007759.
 32. Leo Beranek. Concert halls and opera houses: music, acoustics, and architecture. New York, NY: Springer; 2012. ISBN: 978-0-387-95524-7.
 33. Chatterjee K, Chatterjee K, Kumar A, Shankar S. Healthcare impact of COVID-19 epidemic in india: A stochastic mathematical model. Medical Journal Armed Forces India. 2020; 76(2):147-155. doi: 10.1016/j.mjafi.2020.03.022.
 34. Grant A. Dynamics of COVID-19 epidemics: Seir models underestimate peak infection rates and overestimate epidemic duration. medRxiv. Preprint posted April 12, 2020. doi: 10.1101/2020.04.02.20050674.
 35. He S, Peng Y, Sun K. Seir modeling of the COVID-19 and its dynamics. Nonlinear Dynamics. 2020; 101:1667-1680. doi: 10.1007/s11071-020-05743-y.
 36. Pandey G, Chaudhary P, Gupta, R, Pal S. Seir and regression model based COVID-19 outbreak predictions in india. medRxiv. Preprint posted April 3, 2020. doi: 10.1101/2020.04.01.20049825.
 37. Wu JT, Leung K, Leung GM. Nowcasting and forecasting the potential domestic and international spread of the 2019-ncov outbreak originating in Wuhan, China: a modelling study. The Lancet. 2020; 395(10225). doi: 10.1016/S0140-6736(20)30260-9.
 38. Zhao S, Chen H. Modeling the epidemic dynamics and control of COVID-19 outbreak in China. Quantitative Biology. 2020; 11:1-9. doi: 10.1007/s40484-020-0199-0.
 39. Akbarpour M, Cook C, Marzuoli A, et al. Socioeconomic network heterogeneity and pandemic policy response. NBER Working Paper. Preprint posted June 2020. doi: 10.3386/w27374.
 40. Chang SL, Harding N, Zachreson C, Cliff OM, Prokopenko M. Modelling transmission and control of the COVID-19 pandemic in Australia. Nature. 2020; 11(5710). doi: 10.1038/s41467-020-19393-6.
 41. Kai D, Goldstein G, Morgunov A, Nangalia V, Rotkirch A. Universal masking is urgent in the COVID-19 pandemic: Seir and agent based models, empirical validation, policy recommendations. arXiv. Preprint posted online April 22, 2020. doi: 10.13140/RG.2.2.21662.08001
 42. Rockett RJ, Arnott A, Lam C, et al. Revealing COVID-19 transmission in Australia by SARS-CoV-2 genome sequencing and agent-based modeling. Nature Medicine. 2020; 26(9):1398-1404. doi: 10.1038/s41591-020-1000-7.
 43. Silva PCL, Batista PVC, Lima HS, Alves MA, Guimarães FG, and Silva RCP. COVID-abs: An agent-based model of COVID-19 epidemic to simulate health and economic effects of social distancing

- interventions. *Chaos, Solitons & Fractals*. 2020; 139:110088. doi: [10.1016/j.chaos.2020.110088](https://doi.org/10.1016/j.chaos.2020.110088).
44. Wallinga J, Lipsitch M. How generation intervals shape the relationship between growth rates and reproductive numbers. *Proceedings of the Royal Society B: Biological Sciences*. 2007; 274(1609):599-604. doi: [10.1098/rspb.2006.3754](https://doi.org/10.1098/rspb.2006.3754).
 45. Dietz K. The estimation of the basic reproduction number for infectious diseases. *Statistical Methods in Medical Research*. 1993; 2(1):23-41. doi: [10.1177/096228029300200103](https://doi.org/10.1177/096228029300200103)
 46. He J, Guo Y, Mao, R, Zhang J. Proportion of asymptomatic coronavirus disease 2019: A systematic review and meta-analysis. *Journal of medical virology*. 2021; 93(2):820-830. doi: [10.1002/jmv.26326](https://doi.org/10.1002/jmv.26326).
 47. McAloon C, Collins A, Hunt K, et al. Incubation period of COVID-19: a rapid systematic review and meta-analysis of observational research. *BMJ Open*. 2020; 10(8):e039652. doi: [10.1136/bmjopen-2020-039652](https://doi.org/10.1136/bmjopen-2020-039652).
 48. van Kampen JJA, van de Vijver DAMC, Fraaij PLA, et al. Duration and key determinants of infectious virus shedding in hospitalized patients with coronavirus disease-2019 (COVID-19). *Nature Communications*. 2021; 12:267. doi: [10.1038/s41467-020-20568-4](https://doi.org/10.1038/s41467-020-20568-4).
 49. Kucirka LM, Lauer SA, Laeyendecker O, Boon, D, Lessler J. Variation in false-negative rate of reverse transcriptase polymerase chain reaction-based SARS-CoV-2 tests by time since exposure. *Annals of Internal Medicine*. 2020 173(4):262-267. doi: [10.7326/M20-1495](https://doi.org/10.7326/M20-1495).
 50. Pray IW. Performance of an antigen-based test for asymptomatic and symptomatic SARS-CoV-2 testing at two university campuses—Wisconsin, September-October 2020. *Morbidity and Mortality Weekly Report*. 2021; 69(5152):1642-1647. doi: [10.15585/mmwr.mm695152a3](https://doi.org/10.15585/mmwr.mm695152a3).
 51. Singanayagam A, Patel M, Charlett A, et al. Duration of infectiousness and correlation with RT-PCR cycle threshold values in cases of COVID-19, England, January to May 2020. *Eurosurveillance*. 2020; 25(32):2001483. doi: [10.2807/1560-7917.ES.2020.25.32.2001483](https://doi.org/10.2807/1560-7917.ES.2020.25.32.2001483).
 52. He X, Lau EHY, Wu P, et al. Temporal dynamics in viral shedding and transmissibility of COVID-19. *Nature Medicine*. 2020; 26(5):672-675. doi: [10.1038/s41591-020-0869-5](https://doi.org/10.1038/s41591-020-0869-5).
 53. Donnat C, Miolane N, Bunbury F, Kreindler J. A Bayesian hierarchical network for combining heterogeneous data sources in medical diagnoses. *Machine Learning for Health*. 2020; 136:53-84.
 54. Public Health England. Impact of COVID-19 vaccines on mortality in England: December 2020 to March 2021. 2021. https://assets.publishing.service.gov.uk/government/uploads/system/uploads/attachment_data/file/977249/PHE_COVID-19_vaccine_impact_on_mortality_March.pdf.
 55. World Health Organization. Modes of transmission of virus causing COVID-19: implications for ipc precaution recommendations. 2020. <https://www.who.int/news-room/commentaries/detail/modes-of-transmission-of-virus-causing-covid-19-implications-for-ipc-precaution-recommendations/>.
 56. Morawska L, Milton DK. It is time to address airborne transmission of coronavirus disease 2019 (COVID-19). *Clinical Infectious Diseases*. 2020; 71(9):2311-2313. doi: [10.1093/cid/ciaa939](https://doi.org/10.1093/cid/ciaa939).
 57. Lewis D. Is the coronavirus airborne? experts can't agree. *Nature*. 2020; 580(7802):175. doi: [10.1038/d41586-020-00974-w](https://doi.org/10.1038/d41586-020-00974-w).
 58. Nishiura H, Oshitani H, Kobayashi T, et al. Closed environments facilitate secondary transmission of coronavirus disease 2019 (COVID-19). *medRxiv*. Preprint posted April 16, 2020. doi: [10.1101/2020.02.28.20029272](https://doi.org/10.1101/2020.02.28.20029272).
 59. Asadi S, Bouvier N, Wexler, AS, Ristenpart WD. The coronavirus pandemic and aerosols: Does COVID-19 transmit via expiratory particles? *Aerosol Science and Technology*. 2020; 54(6):635-638. doi: [10.1080/02786826.2020.1749229](https://doi.org/10.1080/02786826.2020.1749229).
 60. Zhang R, Li Y, Zhang AL, Wang, Y, Molina MJ. Identifying airborne transmission as the dominant route for the spread of COVID-19. *Proceedings of the National Academy of Sciences*. 2020; 117(26):14857-14863. doi: [10.1073/pnas.2009637117](https://doi.org/10.1073/pnas.2009637117).
 61. Bhagat RK, Wykes MSD, Dalziel SB, and Linden PF. Effects of ventilation on the indoor spread of COVID-19. *Journal of Fluid Mechanics*. 2020; 903:F1. doi: [10.1017/jfm.2020.720](https://doi.org/10.1017/jfm.2020.720).
 62. Miller SL, Nazaroff WW, Jimenez JL, et al. Transmission of SARS-CoV-2 by inhalation of respiratory aerosol in the Skagit Valley Chorale superspreading event. *Indoor air*. 2021; 31(2):314-323. doi: [10.1111/ina.12751](https://doi.org/10.1111/ina.12751).
 63. Elbanna A, Wong GN, Weiner ZJ, et al. Entry screening and multi-layer mitigation of COVID-19 cases for a safe university reopening. *medRxiv*. Preprint posted September 2, 2020. doi: [10.1101/2020.08.29.20184473](https://doi.org/10.1101/2020.08.29.20184473).

64. Buonanno G, Stabile L, Morawska L. Estimation of airborne viral emission: Quanta emission rate of SARS-CoV-2 for infection risk assessment. *Environment International*. 2020; 141:105794. doi: [10.1016/j.envint.2020.105794](https://doi.org/10.1016/j.envint.2020.105794).
65. Fennelly KP. Particle sizes of infectious aerosols: implications for infection control. *The Lancet Respiratory Medicine*. 2020; 8(9):914-924. doi: [10.1016/S2213-2600\(20\)30323-4](https://doi.org/10.1016/S2213-2600(20)30323-4).
66. Brooks JT, Butler JC. Effectiveness of mask wearing to control community spread of SARS-CoV-2. *JAMA*. 2021; 325(10):998-999. doi: [10.1001/jama.2021.1505](https://doi.org/10.1001/jama.2021.1505).
67. Peebles L. What the data say about wearing face masks. *Nature*. 2020; 586:186-189. doi: [10.1038/d41586-020-02801-8](https://doi.org/10.1038/d41586-020-02801-8).
68. Jimenez. Aerosol transmission model, 2020. Available at <https://docs.google.com/spreadsheets/d/16K1OQkLD4BjgBdO8ePj6ytf-RpPMIJ6aXfg3PrIQBbQ/edit#gid=519189277>, Accessed August 3rd 2021.
69. Harrichandra A, Ierardi, AM, Pavilonis B. An estimation of airborne SARS-CoV-2 infection transmission risk in New York City nail salons. *Toxicology and Industrial Health*. 2020; 36(9):634-643. doi: [10.1177/0748233720964650](https://doi.org/10.1177/0748233720964650).
70. Riley EC, Murphy G, Riley RL. Airborne spread of measles in a suburban elementary school. *American Journal of Epidemiology*. 1978; 107(5):421-432. doi: [10.1093/oxfordjournals.aje.a112560](https://doi.org/10.1093/oxfordjournals.aje.a112560).
71. Wells WF. Airborne contagion and air hygiene. An ecological study of droplet infections. Cambridge, MA: Harvard University Press; 1955.
72. To GNS, Chao CYH. Review and comparison between the wells-riley and dose-response approaches to risk assessment of infectious respiratory diseases. *Indoor Air*. 2010; 20(1):2-16. doi: [10.1111/j.1600-0668.2009.00621.x](https://doi.org/10.1111/j.1600-0668.2009.00621.x).
73. Beare BK, Toda AA. On the emergence of a power law in the distribution of COVID-19 cases. *Physica D: Nonlinear Phenomena*. 2020; 412:132649. doi: [10.1016/j.physd.2020.132649](https://doi.org/10.1016/j.physd.2020.132649).
74. Althouse BM, Wenger EA, Miller JC, et al. Stochasticity and heterogeneity in the transmission dynamics of SARS-CoV-2. *arXiv. Preprint posted May 27, 2020*.
75. Cirillo P, Taleb NN. Tail risk of contagious diseases. *Nature Physics*. 2020; 16(6):606-613. doi: [10.1038/s41567-020-0921-x](https://doi.org/10.1038/s41567-020-0921-x).
76. Obadia T, Haneef, R, Boëlle P. The R0 package: a toolbox to estimate reproduction numbers for epidemic outbreaks. *BMC Medical Informatics and Decision Making*. 2012; 12(1):1-9. doi: [10.1186/1472-6947-12-147](https://doi.org/10.1186/1472-6947-12-147).
77. Kamvar ZN, Cai J, Pulliam JRC, Schumacher, J, Jombart T. Epidemic curves made easy using the r package incidence. *F1000Research*. 2019; 8:139. doi: [10.12688/f1000research.18002.1](https://doi.org/10.12688/f1000research.18002.1).
78. R Epidemics Consortium. Projections. Available from <https://www.repidemicsconsortium.org/projections/index.html>.
79. Noakes CJ, Beggs CB, Sleight PA, and Kerr KG. Modelling the transmission of airborne infections in enclosed spaces. *Epidemiology and Infection*. 2006; 134(5):1082-1091. doi: [10.1017/S0950268806005875](https://doi.org/10.1017/S0950268806005875).
80. Peng S, Chen, Q, Liu E. The role of computational fluid dynamics tools on investigation of pathogen transmission: Prevention and control. *Science of the Total Environment*. 2020; 746:142090. doi: [10.1016/j.scitotenv.2020.142090](https://doi.org/10.1016/j.scitotenv.2020.142090).
81. Rudnick SN, Milton DK. Risk of indoor airborne infection transmission estimated from carbon dioxide concentration. *Indoor Air*. 2003; 13(3):237-245. doi: [10.1034/j.1600-0668.2003.00189.x](https://doi.org/10.1034/j.1600-0668.2003.00189.x).
82. Fennelly KP, Nardell EA. The relative efficacy of respirators and room ventilation in preventing occupational tuberculosis. *Infection Control and Hospital Epidemiology*. 1998; 19(10):754-759. doi: [10.1086/647719](https://doi.org/10.1086/647719).
83. Nazaroff WW, Nicas M, Miller SL. Framework for evaluating measures to control nosocomial tuberculosis transmission. *Indoor Air*. 1998; 8(4):205-218. doi: [10.1111/j.1600-0668.1998.00002.x](https://doi.org/10.1111/j.1600-0668.1998.00002.x).
84. Nicas M. An analytical framework for relating dose, risk, and incidence: an application to occupational tuberculosis infection. *Risk Analysis*. 1996; 16(4):527-538. doi: [10.1111/j.1539-6924.1996.tb01098.x](https://doi.org/10.1111/j.1539-6924.1996.tb01098.x).
85. Schuit M, Ratnesar-Shumate S, Yolitz J, et al. Airborne SARS-CoV-2 is rapidly inactivated by simulated sunlight. *The Journal of Infectious Diseases*. 2020; 222(4):564-571. doi: [10.1093/infdis/jiaa111](https://doi.org/10.1093/infdis/jiaa111).

[10.1093/infdis/jiaa334](https://doi.org/10.1093/infdis/jiaa334).

86. Dabisch P, Schuit M, Herzog A, et al. The influence of temperature, humidity, and simulated sunlight on the infectivity of SARS-CoV-2 in aerosols. *Aerosol Science and Technology*. 2021; 55(2):142-153. doi: [10.1080/02786826.2020.1829536](https://doi.org/10.1080/02786826.2020.1829536).
87. Parliament of the United Kingdom. Call for evidence in COVID-19 certification inquiry. 2021. <https://committees.parliament.uk/committee/327/public-administration-and-constitutional-affairs-committee/news/153049/call-for-evidence-in-covid19-certification-inquiry/>.
88. Home COVID test. Available at https://homecovidtests.shinyapps.io/aerosol_transmission_model/ [accessed August 3, 2021].
89. Revollo, Boris, et al. "Same-day SARS-CoV-2 antigen test screening in an indoor mass-gathering live music event: a randomised controlled trial." *The Lancet Infectious Diseases* (2021). doi: [https://doi.org/10.1016/S1473-3099\(21\)00268-1](https://doi.org/10.1016/S1473-3099(21)00268-1)
90. Llibre, Josep M., et al. "Screening for SARS-CoV-2 antigen before a live indoor music concert: an observational study." *Annals of Internal Medicine* (2021). doi: 10.7326/M21-2278
91. Swinkels, K. (2020). SARS-CoV-2 Superspreading Events Around the World [Google Sheet]. Retrieved from www.superspreadingdatabase.com.
92. Donnat, Claire, and Susan Holmes. "Modeling the heterogeneity in COVID-19's reproductive number and its impact on predictive scenarios." *Journal of Applied Statistics* (2021): 1-29. doi: 10.1080/02664763.2021.1941806
93. Cirillo, Pasquale, and Nassim Nicholas Taleb. "Tail risk of contagious diseases." *Nature Physics* 16.6 (2020): 606-613. doi: 10.1038/s41567-020-0921-x
94. COVID event risk survey Available at https://docs.google.com/forms/d/e/1FAIpQLSfCqmEltbJtOhfVTd_yNvhu4t0yulyAziuxStGXx8YI0MVQ0w/viewform?usp=sf_link [accessed August 16, 2021].

Appendix A: Prediction

As explained in the introduction, the aim of this paper is to develop a context-aware risk model. To be informative, the estimates of the risk that the model outputs must be informed by (a) the prevalence at the time of the event, (b) the ticket holders' vaccination status, and (c) the screening protocol employed by the event management to reduce transmission risk. In this setting, the CAPACITY protocol serves as a case in point and a motivation to our paper. Central to the study is the estimation of the risk associated with the event on two different horizons:

Horizon 1: Weeks prior to the event. In this setting, the goal is to predict ahead of time the risk associated with the event, so as to help organizers and participants alike to plan ahead and decide whether or not they deem the risk associated with the event acceptable. *This step requires the prediction of both the prevalence of the disease and the vaccination status of the crowd several weeks in advance.*

Horizon 2: A few days before the event. The purpose of the risk estimation is to evaluate – with more certainty – the admissibility of the risk associated with the event. In this step, *the algorithm can rely on ticket holders' reported vaccination status, as well as the most recent incidence rates to compute the risk.* This allows in particular to reduce the uncertainty in the prevalence rate substantially, and circumvents the problem of imputing prevalence and vaccination status.

Thus, *whilst not crucial for Horizon 2 (in the last few days leading up to the event), the prediction of the crowd's vaccination status as well as the incidence rate are major components of Horizon 1* – thereby calling for prediction methods that both provide accurate estimates and a correct evaluation of their associated uncertainty. In this appendix, we focus on providing more details into the different predictive components that we use to estimate the risk ahead of time (Horizon 1). These consist of the following three main steps, which we subsequently describe in greater details:

- **Step a:** The prediction of the number of newly infected individuals who are ticket holders.

- **Step b:** The prediction of the number of infected participants that will escape the screening protocol.
- **Step c:** The prediction of the number of vulnerable ticket holders at the time of the event (i.e., participants that are not immune).

Step a. Prediction of new cases through a k-Nearest Neighbour (k-NN) Approach. The first step in our pipeline consists of the estimation of the daily incidence rate in the days leading to the event, which, in the main text of this paper, we suggested solving using a k -nearest neighbour approach with $k=100$. Specifically, we consider the trajectories of the daily incidence rate (per million) over all countries, and across different points of the epidemic on intervals of $D_{train}=14$ days. This creates a “dictionary” of over 30,000 observed epidemic-kinetics behaviours. We then determine the l_2 distance between the last $D_{train}=14$ days of the trajectory of interest (that is, the trajectory for which we want to predict the next $D_{predict}$ days) and all fourteen-day historical trajectories in our dictionary. We then retain the closest $k=100$ neighbours (corresponding to the smallest l_2 distance), and translate them appropriately so that their last day of fitting matches the last value recorded in our trajectory of interest. We summarize these $k=100$ trajectories to get a prediction and prediction interval for our trajectory of interest: we use the mean, 2th and 98th quantiles of the historical trajectories of the 100 closest neighbours over $D_{predict}$ days to predict the expected incidence rate and provide a prediction interval for the next $D_{predict}$ days. The procedure is summarized in Algorithm 1.

The choice of $k=100$ neighbours allows us to have sufficient information to evaluate the percentiles of the distribution of the prediction, whilst retaining a sufficient amount of similarity with the original trajectory. The choice of 14 days is motivated by the fact that we need sufficient data to find trajectories with similar behaviours, whilst remaining sufficiently local for the comparison to be valid: epidemic kinetics change from month to month, or even week to week, so the similarity in epidemic kinetics might only hold for a limited time frame. We provide more details on the selection of these parameters, as well as compare this method against more commonly used benchmarks in the subsequent paragraph.

Data: Previous Incidence data $Y \in \mathbb{R}^{n \times T}$;
 Choice of $k=100$;
 Input vector $X \in \mathbb{R}^{p_{train}}$ with p_{train} the length of the training period;
 p_{pred} the desired length of prediction period;
Result: k-Nearest Neighbors sample trajectories of length p_{pred} , average prediction and uncertainty estimates

Step 1: Compute the distance matrix:

```

for i in 1:n do
  for t in 1:T by 14 do
    Compute distance:  $D_{[t/14]J+1,i} = \text{distance}(X, Y_{(t-p_{train}+1):t})$ ;
  end
end
```

end

Step 2: Extract k nearest neighbours:

I, J = Row and Column Indices of the k-smallest elements of D;

Step 3: Recenter (translate) the prediction on start date to start the predicted trajectory:

$\hat{Y}[1:p_{pred}] = \text{Mean } \hat{z}$;

Algorithm 1: Prediction of the epidemic curve using k-NN

Motivation for the k -NN approach. COVID-19 prediction is undoubtedly an involved task — as denoted by the impressive amount of literature published on the topic [34, 35, 36, 37, 38, 39, 40, 41, 42, 43, 44]. Yet, as emphasized in the main text, many of these methods rely on a parametrization of the problem (Exponential growth, SEIR model, etc. [45, 46]) which require input parameters (e.g., the reproductive number) that are both unknown and non-stationary. Indeed, as the number of cases rises, policy makers are bound to adapt their policies to limit the spread of the virus. Reciprocally, as community prevalence levels drop, strict lockdown measures and stay-at-home orders are bound to be lifted — thus impacting the transmission modalities and likelihood of propagation of the virus.

Incorporating both uncertainty and non-stationarity in COVID predictions is thus a challenging task. Our solution to this problem relies on using a fully non-parametric, **model-agnostic k -Nearest Neighbour (k -NN) approach**: this approach essentially predicts the behaviour of the incidence rate (normalized per million people) using historical data. We argue that such a non-parametric approach to fit growth epidemic curves has the potential to be more accurate than other parametric models that (a) rely on a specific sets of assumptions (ie, compartmental models), (b) are only valid for a limited amount of time (e.g, Exponential Growth models), and (c) assume a stationary, identical regime of growth/ public policy throughout their predictions. By contrast, historical trajectories contain information both on the reproductive number and propensity of the epidemic to grow, but also on policy decisions made as a result of rising (or declining) prevalence numbers — thus making them an appealing non-parametric candidate for non-stationary incidence modelling.

Selection of the k -NN parameters. While k -NN is a non-parametric, model agnostic approach that does not make any assumptions on epidemic kinetics nor effects of public policy attempting to curb the spread, it requires nonetheless the selection of three critical parameters: (1) The similarity function to determine the nearest neighbours, (2) the number of nearest neighbours k , as well as (3) the number of days D_{train} used for training. In the previous two paragraphs, we detailed the k -NN procedure providing the values of the parameters that we use in our final algorithm. This selection stems in fact from the results of a grid-search over candidate values for both k , D_{train} , and the similarity function:

- **Similarity function:** The choice of the distance function that determines the resemblance between two incidence trajectories is a crucial component of the algorithm. We compare the use of four similarity functions:
 - **Simple MSE.** In this case, denoting $X_i, X_j \in R^{D_{train}}$ two incidence trajectories, their similarity is simply

given by: $s_{ij}^{MSE} = \frac{1}{D_{train}} \sum_{t=1}^{D_{train}} (X_{it} - X_{jt})^2$. We refer to this distance as the “Mean Squared-Error” (MSE).

- **Weighted MSE.** To place more weight on matching the most recent observations in the trajectories, we consider a version of our MSE metric in which the weights of observations are inversely proportional to the time since the origin of prediction (i.e., for each day $k \in [1, D_{train}]$, $w_k = \frac{1}{D_{train} + 1 - k}$), so that:

$$s_{ij}^{W-MSE} = \sum_{t=1}^{D_{train}} \frac{1}{D_{train} + 1 - t} (X_{it} - X_{jt})^2.$$

This weighting puts more emphasis on recent observations, so that trajectories that share a higher degree of similarity in their recent behaviours will be favoured by the algorithm. We will denote this method by “Weighted Mean Square Error”.

- **Correlation.** Another way of measuring similarities between distributions consists in using a correlation measure between trajectories, so that the distance between two trajectories is simply:

$$s_{ij}^{corr} = 1 - \sum_{t=1}^{D_{train}} \frac{(X_{it} - \bar{X}_i)(X_{jt} - \bar{X}_j)}{\|X_i\| \|X_j\|} = 1 - \text{corr}(X_i, X_j). \text{ Compared to the MSE metric, this measure}$$

only considers the shape and direction of increase, but does not consider information in the actual value of the incidence itself: contrary to the MSE, this measure encourages matching rates of increase, regardless of the incidence rate in one curve is above 500 in one curve, and 10 in the other – vastly different COVID regimes, that can potentially yield very different public policy measures as a response.

- **Weighted Correlation.** This distance is an extension of the correlation-based distance, which gives more weight to recent observations (in a similar manner than for the “Weighted- MSE”). The distance between

two trajectories is simply: $s_{ij}^{w-corr} = 1 - \sum_{t=1}^{D_{train}} \frac{1}{D_{train} + 1 - t} \frac{(X_{it} - \bar{X}_i)(X_{jt} - \bar{X}_j)}{\|X_i\| \|X_j\|}.$

- **Determining the k in k-NN:** The estimation of the percentiles for the distribution requires us to have at least 100 nearest neighbours. However, the choice of the number of neighbours is subject to the classical “bias versus variance” trade-off: as k increases, the bias of the model also increases, as we might be using trajectories that are too different to be useful. In our grid-search, we thus use {100, 200, 300, 500} as candidate numbers of curves to do our predictions.
- **Determining the length of the training period:** Similarly, the length of the training set (that is, the number of days that we use to find “nearest historical trajectories”) is also “subject to a bias versus variance” tradeoff: epidemic kinetics are rapidly varying, and change from month to month, or even week to week. As such, the selection of the appropriate length for our fitting window must arbitrate between being short enough to capture recent epidemic developments, but sufficiently long to correctly capture similar behaviours. To determine this parameter, we also use a grid-search approach, allowing the training window to vary between {7, 14, 21, 28} days.

Benchmarking of the k-NN approach. To provide more substantial ground for our proposed k-NN approach, we studied its performance compared to more traditional benchmarks using exponential growth model and Attack rate models [46, 45], commonly used in the literature and implemented in the R package R0 [77].

Grid-search and benchmark experiments. We compute the performance of each method and vary the similarity, k , and length of training period to establish the optimal set of parameters. To summarize and be fully explicit, our comparison thus focuses on comparing:

- The Attack Rate method [45], using the R packages R0 [77], Incidence [78] and Projections [79],
- The Exponential Growth model [46] (using the same R packages),
- Our k-NN method with MSE distance, W-MSE, correlation or W-Corr distances.
- Our k-NN method with an MSE distance, but computing the prediction using the median of the k -nearest neighbours rather than the mean.

To compare these methods, we use data from "Our World in Data": for each country, we evaluate the performance of each method for predictions between June 1st 2020 to July 1st 2021. Every two or three months (depending on the rapidity of the spread: June 1st 2020, September 1st, November 1st, January 1st 2021, March 1st, July 1st), we recreate a prediction scenario. We use {7, 14, 21, 28} weeks of observations for training, and predict the daily incidence for the next four weeks (28 days). The purpose of this experiment is to assess and compare across methods (a) the methods' prediction accuracy, and (b) the coverage (percentage of times that the confidence interval covers the true observations), in order to establish which method allows to correctly estimate the uncertainty and risk. Figure 6 presents a comparison of statistics of the Weighted Root Mean Square Error (W-RMSE, defined as

$\sqrt{\sum_{t=1}^{D_{pred}} \frac{1}{D_{pred} + 1 - t} (\hat{X}_{it} - X_{it}^{obs})^2}$), averaged over all countries and all dates (top panel) and for the 95th percentile of the W-RMSE, showing how robust and well-behaved these predictions are (bottom panel). From these graphs, we can clearly see the bias versus variance effect trade-off effect in the number of curves: the accuracy decreases (as denoted by an increase in RMSE) as the number of k -nearest neighbour curves used for the prediction increases. Similarly, predictions are less accurate for longer fitting windows. Overall, we observe the superior performance of the MSE method – that is, when using the MSE as a similarity score, and using the median of k nearest neighbours (instead of the mean) to do the prediction. In particular, a choice of $k=100$ for a training window of 14 days seems to provide the best results (best mean and 95th quantile) – see Figure 6 and Table 2.

| Method | Training Window Length | Number of Closest Neighbours | Mean W-RMSE | Median W-RMSE | 95 th Quantile of W-RMSE | Mean Width of the Prediction Interval |
|-------------|------------------------|------------------------------|-------------|---------------|-------------------------------------|---------------------------------------|
| Median-MSE | 14 | 200 | 41.1 | 8.67 | 202.0 | |
| W-MSE | 14 | 100 | 39.9 | 9.53 | 186.7 | |
| MSE | 14 | 100 | 39.7 | 9.57 | 183.3 | |
| Correlation | 7 | 100 | 47.3 | 9.71 | 244.0 | |

| | | | | | | |
|--------------------|----|-----|------|-------|-------|--|
| W-Correlation | 7 | 500 | 48.2 | 9.83 | 250.4 | |
| Attack Rate | 21 | | 55.2 | 11.70 | 264.4 | |
| Exponential Growth | 28 | | 67.8 | 20.47 | 1815 | |

Table 2: Summary for the goodness of fit tests on the test data. Results correspond to the mean, median and 95th quantile of the W-RMSE over all dates and all countries in the test data. We show the best performing model from each category. We note the clear superiority of the kNN neighbour method over the Attack Rate and Exponential Growth model: the MSE based classification model achieves a reduction in W-RMSE of respectively 28% and 41%.

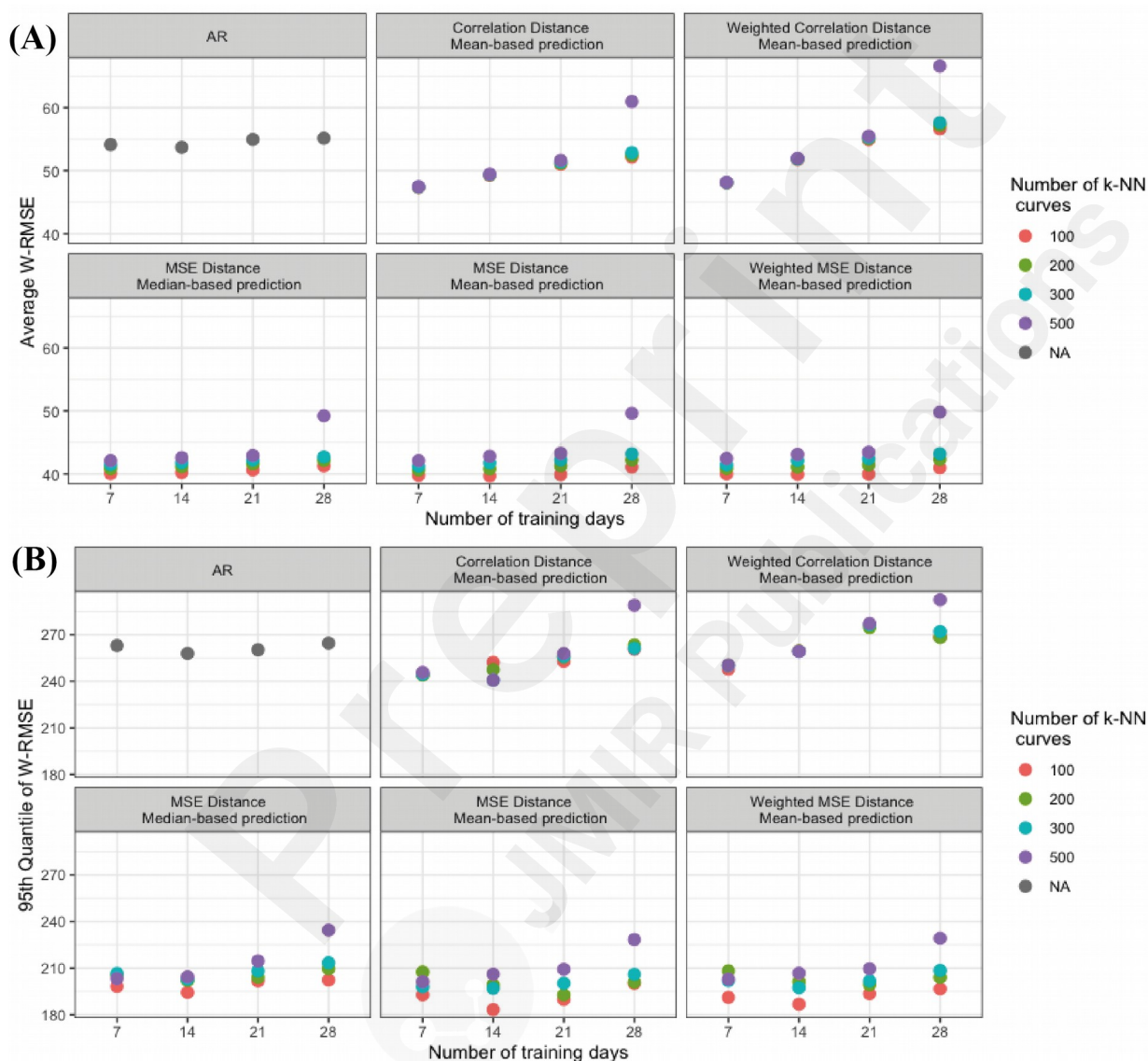


Figure 6: Weighted Root Mean Square Error for the different methods (mean and 95th quantile). We note the robustness of the mean and median based-MSE to the fitting window length.

The results across countries and periods are provided in Figure 6, displayed for a subset of countries on Figure 7 and the coverage is shown in Figure 8. We see that the k-NN method achieves comparable weighted Root Mean Square Error (W-RMSE) to the classical projection methods implemented in R. Yet, the k-NN method also achieves a coverage of more than 90% (and close to the nominal 95% that it targets), and the prediction interval that it provides is thus more reliable than that of other methods.

Under-ascertainment bias. Having predicted the daily incidence rate in the weeks leading to the events, to correctly estimate the number of ticket holders that are likely to be contaminated, it is important to correct this prevalence estimate for any under-reporting bias. The under-ascertainment bias refers to the fact that the reported COVID cases

are in fact an under-estimation of the actual number of cases, due to either

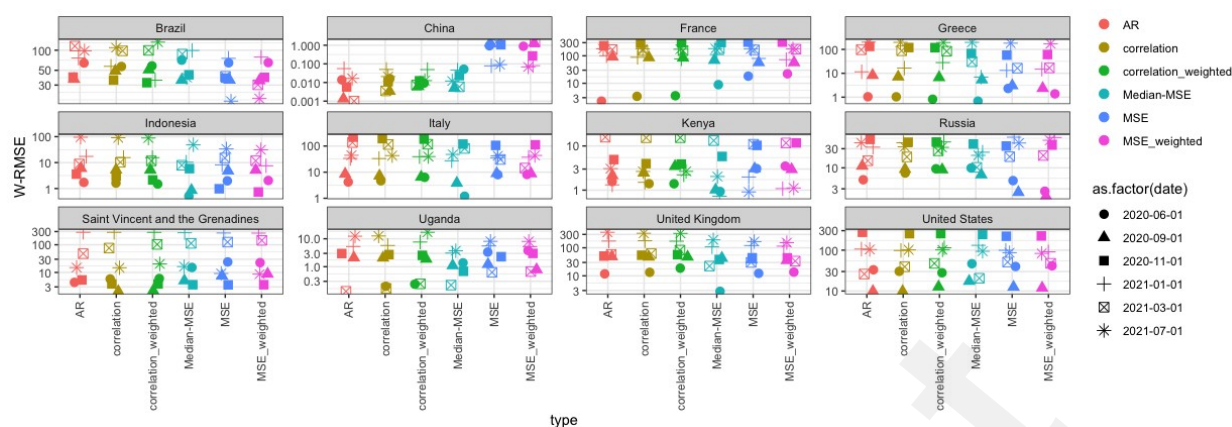
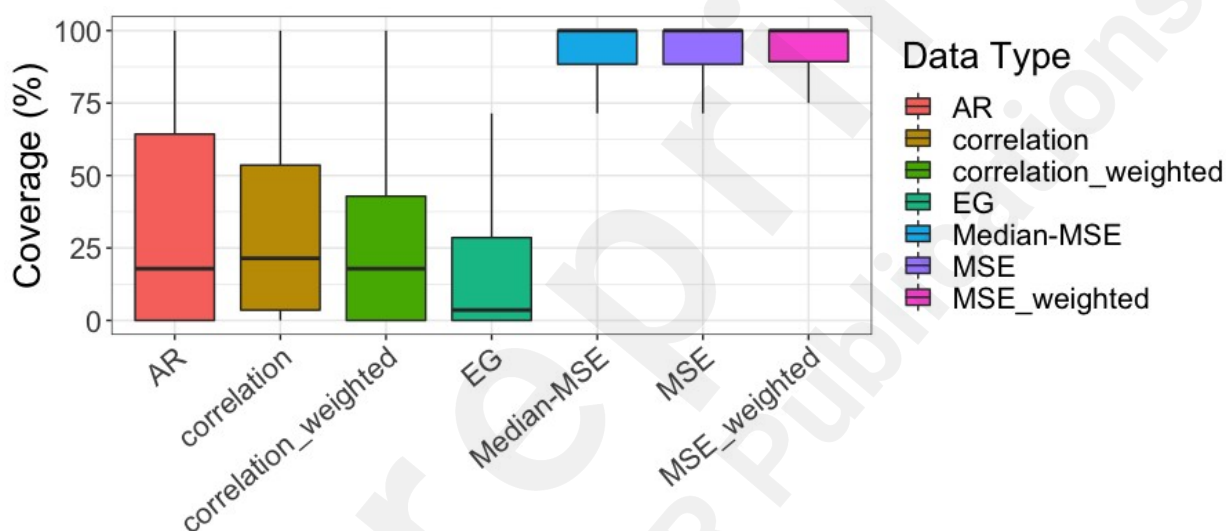


Figure 7: Performance of the different methods for predicting the epidemics trajectories (subset of countries around the world). The MSE performs the best on average and according to 95th percentile, but there are differences in performance across time and countries.



Figure

8: Performance of the different methods for predicting the epidemics trajectories (subset of countries around the world) for coverage

asymptomatic cases or limited testing capacities. In order to compute the appropriate correction, we use age-stratified estimates of the Infection-Fatality rate⁴. The method provided at this link has the advantage of computing robust IFR estimates by leveraging data from countries around the world, and adjusting for their demographic makeup. The actual number of cases is then computed as:

$$\text{bias}[t - \text{lag}] = \frac{\text{cases}[t - \text{lag}]}{\text{deaths}[t]} \times \text{IFR}$$

Indeed, since deaths are offset compared to the incidence rate, reported new cases must be compared to deaths roughly three weeks later (according to CDC reports). The under-ascertainment in the case of Britain is plotted in Figure 6a.

Step b. Estimating the Number of People who will escape the screening protocol. For the sake of clarity and to make this appendix self-contained, we repeat here the discussion of the screening protocol provided in the main text,

⁴ The IFR have been taken from the following data source: <https://github.com/mbevand/covid19-age-stratified-ifr>

but provide additional detail on the estimation procedure. For an infectious individual to attend the event in spite of the CAPACITY study's screening protocol, they must (a) have no COVID-like symptoms or fail to report them on the morning of the event, (b) receive a (false) negative result during antigen testing $D = 2$ days prior to the event, and (c) be contagious (rather than simply infected) at the time of the event.

(i) *Symptoms-Check Failure.* Indeed, one of the main challenges associated with the COVID-19 crisis is the number of asymptomatic cases - that is, infected individuals that do not express symptoms and are thus unaware of their potential infectiousness. This group encompasses people that are either pre-symptomatic or completely asymptomatic during the course of their illness - the latter are estimated to represent roughly 25% of all cases [47]. To account for this temporal dependency, we use estimates of the incubation period (defined as the number of days between infection and symptom onset) from McAloon et al. [48] and data on symptoms duration from van Kampen et al. [49] to estimate the probability for a ticket holder infected s days before the event to exhibit symptoms on the day of the event. We rely on simulations to estimate this probability distribution, finding estimates of the time to symptom onset by randomly generating an incubation period using data from McAloon et al. [48], and sampling a symptom duration from van Kampen et al. [49]. The resulting density plot is displayed in red in Figure 3a.

(ii) *Antigen test failure.* The sensitivity of COVID tests depends heavily on the time since infection, and whether these are the gold-standard PCR or Lateral Flow Antigen Assays [50]. Moreover, studies have shown that LFA tests have much lower sensitivity on asymptomatic individuals than symptomatic: in particular, according to a recent CDC report [51], Rapid Antigen testing has 80% sensitivity on symptomatic individuals, but only 40% sensitivity on asymptomatic individuals. Coupling the sensitivity estimates [50, 51] with the distribution of incubation period and estimated percentage of asymptomatic cases [48, 47], for each individual infected at day k taking an antigen test D days before the event, the probability of getting through the filtering protocol is thus given by the formula:

$$P[\text{Protocol fails} | \text{Contaminated at time } k] = \left(1 - s_{t-k-D}^{(\text{symptomatic})}\right) \left(p_{SC} \times p_{t-k}^{(\text{symptom})} + \left(1 - p_{t-k}^{(\text{symptom})}\right)\right) + p^{(\text{asymptomatic})} \times \left(1 - s_{t-k-D}^{(\text{asymptomatic})}\right)$$

where $s_{t-k-D}^{(\text{symptomatic})}$ and $s_{t-k-D}^{(\text{asymptomatic})}$ are respectively the sensitivities of the test taken D days before the event for a symptomatic participant infected $t-k$ days before the event and an asymptomatic individual. The parameter $p_{t-k}^{(\text{symptom})}$ denotes the probability for a symptomatic individual to exhibit symptoms $t-k$ days after infection, whereas $p^{(\text{asymptomatic})}$ is the probability of being asymptomatic. Finally, the variable p_{SC} denotes the probability of the Symptoms Check failing - namely, that the participant does not want to report their symptom. Currently, this probability is set by default in our model to 50%, and we provide in our interactive dashboard the option to choose other levels. As the CAPACITY study gathers more behavioural data on the participants, we hope to improve this estimate. However, we study the sensitivity of our analysis to the choice of this variable in Appendix C, and show that in view of the total uncertainty surrounding other parameters in the model, the choice of this parameter does not severely affect the robustness of the results.

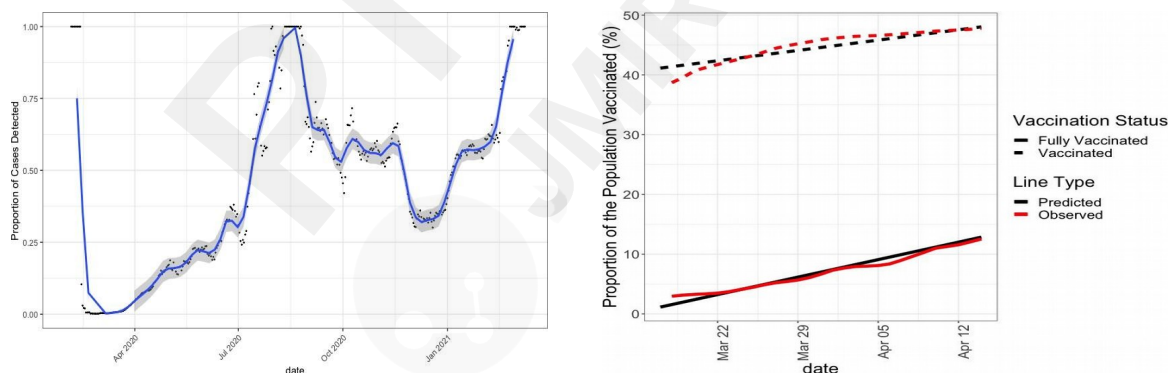
Figure 3b in the main text shows the probability of the failure of the screening protocol as a function of days after infection. This curve was also simulated by sampling: we model the uncertainty in the sensitivity through a set of Monte Carlo simulations, in which, for each simulation: (a) we sample a random sensitivity from a beta distribution, with parameters chosen to match the uncertainty intervals provided in [50], and (b) associate these random sensitivity to the probability of having symptoms and failing to report them. The shaded areas in Figure 3b denote the uncertainty around this estimate due to the variability of the incubation time.

(i) *Estimating Infectiousness.* Infectiousness is a function of time since infection. Many articles in the literature have in particular estimated infectiousness to be at its peak within the first five days after symptom onset. However, very few reports provide an in-depth description of infectiousness as a function of time since infection. To this end, in this paper, we combine data from multiple sources. In particular, we rely on the data from Singanayagam et al [52]. Indeed, in this article, the authors study infectiousness as a function of time since symptom onset which they estimate by looking at the percentage of viable cultures that they can obtain from samples collected at various intervals before and after symptom onset. Since our goal is to consider infectiousness as a function of time since infection (rather than symptom onset), we combine this data with the estimated distribution of incubation length (duration between the date of infection, and date of symptom onset). One of the main issues in converting the data from [52] lies in the long tails of this distribution, which extrapolates from the data and allows samples to be highly contagious up to 10 days before infection. Since Singanayagam et al [52] have very few cases past 4 days prior since infection, we threshold infectiousness to 0 to be consistent with the estimates by He et al [53]. We compound the distribution of incubation and infectiousness by a probability of the incubation length, yielding a probability of infectiousness s days after infection such that:

$$\text{Infectiousness}_s = \sum_{i=1}^{\max(15, s-1)} P[\text{Incubation period} = i \text{ days}] P[\text{Live culture at day } s-i]$$

(ii) **Step c: Estimating the number of people at risk.** Finally, the last quantity that we need to impute is the number of people at risk during the event. As described in the main text, this requires a knowledge of the participants' COVID immunization status, i.e., has the participant already had COVID in the previous year and/or has the participant been vaccinated. This immunization status could be imputed through the combination of information regarding vaccination status as well as additional questions (previous positive test for COVID, symptoms, etc., combined in a model such as in [54]). However, for the sake of simplicity, we only consider here the vaccination status of the participants - thus leaving out the proportion of the population that has had COVID but has not been vaccinated yet. This induces a risk estimate that is biased upward — that is, we do not account for the immunity naturally gained by ticket holders through COVID infection — and as such, is more conservative. When imputing the risk for Horizon 1 (a few weeks before the event, and without any ticket holders' information), we impute the event's crowd immunity level using linear regression. In other words, we assume that the number of new vaccinations (first and second dose) grows linearly each day, which amounts to assuming that vaccinations are operating at capacity. Figure 7 shows a plot of the cumulative number of first and second doses in the UK as a function of time, highlighting a good fit between the linear model and the actual observations. We note though that as vaccination levels are increasing, the linear model will potentially have to be modified: after a certain proportion of the population has been vaccinated, vaccinations could stop operating at capacity since the remainder of the population could either have difficulties in gaining access to the vaccine, or could be opposed to the vaccine altogether. However, at the time of writing, the linear fit seems to be a good fit. Having imputed the rate of new vaccinations $\pi_{s=1\dots t}$ in the days leading to the event, we turn to the estimation of the number of individuals that are likely to be susceptible. Recent reports indicate that vaccine-acquired immunity is a function of both time since vaccination and number of doses [55]. To compute the effective number of participants at risk in the event, we use a compound Poisson distribution: on each day s in the weeks leading to the event, the number X of new participants vaccinated (having either their first or second dose) is expressed as a Poisson($\pi_s^{(\text{dose } j)}$), where $j \in 1, 2$. Each of these newly vaccinated individuals then has a probability $\rho_{t-s}^{(\text{dose } j)}$ of being immune, depending on the date and dose j that they have received. The resulting number of immune people Z attending the event thus follows a Poisson model with rate $Z \sim \text{Poisson}\{\lambda\}$.

However, as the number of vaccination increases, we expect the probability of the participants being immune to increase. In this case, we simply replace the Poisson binomial with a binomial, for various values of $\rho_{t-s}^{(\text{dose } j)}$ to allow the uncertainty around immunity to percolate through the model.



(a) Ascertainment rate for the United Kingdom. The y-axis denotes the ratio of detected cases to cases predicted by multiplying a 3-week shifted death rate by a calculated infection-fatality rate for the U.K. When the values are less than one it suggests that many of the actual cases are not being detected, and when the values are greater than one it suggests that either a substantial proportion of cases are false positives or that survival from COVID infection has increased from baseline predictions, due to better treatments or a greater bias towards infection of individuals at lower risk of death.

(b) Vaccination rate: comparison of the actual rates, and the ones predicted by a linear model for the United Kingdom. The vaccination rates (both first and second dose) seem to be well approximated by a linear regression model (using time as a covariate), with an associated R^2 of 0.92. As time progresses, and vaccination rates increase, this linear fit might start becoming less accurate, as problems of vaccination hesitancy or difficulty to access might induce vaccine centers to operate under capacity.

Figure 9: Under-ascertainment rate (left) and vaccination rate (right) in the United Kingdom.

Appendix B: Transmission

In this appendix, we describe in greater details the model and assumptions made by the Jimenez aerosol transmission model proposed in [69, 63] and used to model transmission dynamics in the main text.

The issue of COVID transmission. As discussed in the main text, the precise mechanisms by which COVID-19 is transmitted are still unclear. Aside from direct physical contact, experts continue to debate the significance of the following two main routes of infection:

(a) *Droplet transmission.* In this scenario, transmission happens through the inhalation of droplets (particles of 5 to 10 μm in diameter [56]), and typically occurs when a person is in close proximity (within 1 meter) with someone who has respiratory symptoms (e.g., coughing or sneezing). In the context of live events, modelling this specific transmission route involves (a) modelling the distribution of the number of close contacts between infectious and susceptible ticket holders during the event and (b) modelling the transmission probability for each close contact. The latter is a function of the proximity between participants and the amount of time spent in the vicinity of the infectious individual.

(b) *Airborne transmission.* Increasing concerns around airborne transmission have been raised by a number of experts over the past few months [57, 58]. Airborne transmission refers to the presence of the virus within droplet nuclei remaining in the air for long periods of time and with the potential to travel long distances [57] and penetrate more deeply in respiratory tracts. Airborne transmission has been estimated to be nearly 19 times more likely indoors than outdoors [59]. In the context of large public events, this transmission route thus has more diffusive power and hence could explain several super-spreader events (SSEs) [6] making it a major cause for concern [60, 61, 53, 62, 2, 57, 63, 64, 65, 66]. In this setting, infection risk is typically modelled using one of two distinct models: Wells-Riley equations and the dose-response model [80, 73]. First introduced by Riley in 1978 in a study of measles outbreak [71], the Wells-Riley equations are based on the concept of a hypothetical infectious unit called a "quantum of infection" [72], defined as the number of infectious airborne particles required to infect a person. Quanta aim to capture in a single parameter the rate of emission of viral particles in exhaled breath, the infectivity of the viruses upon emission, the particle size distribution of the emissions, the deposition efficiency and deposition location in the respiratory tract of the susceptible person, as well as the probability that deposition leads to infection. The dose-response model aims to describe more directly the effect on organisms from the exposure to different doses of chemicals, drugs, radiation, biological agents, or other stressors — and more recently to assess the infection risk of airborne transmissible pathogens. The review by Sze To et al [73] provides an in-depth comparison of the two models. In the context of COVID transmission, one of the main limitations of the dose-response model is that it relies on infectious dose data to derive the dose-response relationship. By contrast, many of the parameters in the Wells-Riley equation can be approximated and has thus been favored by many experts in the field [63, 70].

Choice of Transmission Route for this Model. While droplet emission is undeniably a source of concern and a major source of transmission, simple safety precautions such as mask wearing have been shown to efficiently control this transmission source [67, 68]: it is estimated that face masks can block 80% of exhaled droplets and reduce inhaled droplets by up to 50%, and so on average reduce the transmission probability by 70%. Conversely, the evidence concerning the efficiency of standard protective equipment in filtering aerosol droplets varies widely across studies probably due to "variation in experimental design and particle sizes analyzed" [67]. Airborne transmission in indoor settings can thus represent one of the main risk factors in live events, which we focus on modelling using the aerosol model proposed by Jimenez [69, 63]. The Jimenez aerosol transmission model [69, 81, 63] is indeed currently one of the only COVID-transmission models that provides enough granularity to quantify the risk associated with an event. This recognized model has been used several times in the literature over the course of the pandemic, including to allow in-class teaching at the University of Illinois at Chicago [64]. Based on the Wells-Riley model [72], this estimator calibrates the quanta to known transmission events, and takes into account important factors to compute a risk estimate, including event-specific (number of people, local prevalence, etc.) and venue-specific variables (ventilation rate, size of the venue, UV exposure).

A core principle behind the Wells-Riley model is the notion of "quantum of infection". Exposure to one quantum of infection gives an average probability of $63\% = 1 - e^{-1}$ of becoming infected (essentially an infectious dose 63%, ID₆₃) [82]. The crux of the Wells-Riley equation consists of its modelling of the probability of infection P_I as a function of the ventilation, inhalation rates and quanta generation rates:

$$P_I = 1 - e^{-\frac{I_0 q p t}{Q}} \quad (A)$$

where n_i is the number of infectors, p is the pulmonary ventilation rate of a person, q is the quanta generation rate, t is the exposure time interval, and Q is the room ventilation rate with clean air. Note that this equation is not dimensionless. As explained by Rudnick and Milton [82], q represents the generation rate of infectious doses, not organisms or infectious particles; it is the average infectious source strength of infected individual. Thus, the exponential form of the probability equation reflects the probability of a susceptible person in the room inhaling at least one quanta, based on a Poisson distribution of the number of discrete quanta inhaled by a susceptible person present in the space, given a certain aerosol quanta concentration in the room and an inhalation time.

One of the advantages of the Wells-Riley model is that many extensions have been studied, allowing the incorporation of additional influencing factors. In particular, the effect of respiratory protection can be considered by multiplying the term in the exponential by a fraction [83, 84, 85]:

$$P_I = 1 - \exp\left\{-R \frac{Iqpt}{Q}\right\} \cdot i$$

where R is a number between 0 and 1 representing the fraction of particle penetration of the respiratory protection (it is in particular equal to 1 when no respirator is used). Other variables, such as the ultra-violet irradiation, particle filtration have been taken into account in the Wells-Riley equation through the equation:

$$P_I = 1 - \exp\left\{\frac{-Iqpt}{Q + \lambda_{UV}V + Q_r\eta_r}\right\} (i * i)$$

where λ_{UV} is rate coefficient of inactivation by ultraviolet irradiation, V is the room volume, Q_r is the flow rate to the filter, and η_r is the filtration efficiency.

As suggested by Jimenez et al [69, 63], instead of modelling each of parameters in the Wells Riley equation explicitly, we can use the concept of quanta, and calibrate the emission rate to known outbreaks of the disease. We base the following description of the model as detailed by Jimenez et al [69, 63]. This model relies on the computation of three main components:

1. The Quanta Emission Rate. The quanta emission rate can be interpreted as the number of quanta emitted by unit of time by a single infectious participant. It can be modelled as:

$$q_e = \text{Quanta Exhalation Rate} \times (1 - \text{Mask Efficiency} * P[\text{Wear Mask}]) \times n_{\text{infectious}}$$

2. The Quanta Concentration Rate. The quanta concentration rate q_c is computed as:

$$q_c = \frac{q_e}{\text{Loss} \times \text{Volume}} \times \left(1 - \frac{1}{\text{Loss} \times \text{Duration}} \times (1 - \exp\{-\text{Loss} \times \text{Duration}\})\right)$$

where q_e is the quanta emission rate and $n_{\text{infectious}}$ is the number of infectious people at the event. The loss corresponds to the first order loss:

$$\text{Loss} = \text{Decay} + \text{Ventilation Rate with outside} + \text{Deposition Rate to surfaces} + \text{Additional Control Measures}$$

The term "Decay" corresponds here to the decay rate of the virus, and is a function of the UV, temperature, and relative humidity of the event. The Decay rate per hour is computed according to the following formula [86, 87] for which an open-source calculator is available online⁵:

$$\text{Decay} = \left(7.57 + 1.41 \times \frac{T - 20.54}{10.66} + 0.022 \times \frac{RH - 45.24}{28.67} + 7.55 \times \frac{0.185 \times UV - 50}{50} + \frac{T - 20.54}{10.66} \times \frac{0.185 \times UV - 50}{50}\right)$$

where T is the temperature and UV is the UV index. The tool is valid for the following ranges of conditions: 10 to 30°C (50-86°F), 20-70% relative humidity, and UV indices of 0-10. For live events in an indoor setting, the UV parameter should be set to 0.

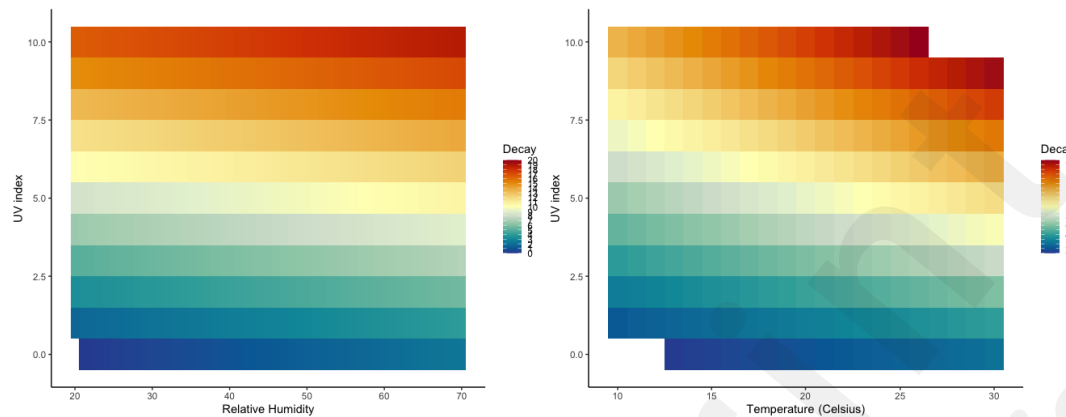
⁵ This calculator can be found at the following link: <https://www.dhs.gov/science-and-technology/sars-airborne-calculator>

We have checked that our computations are aligned with the figures provided in the references.

3. The Quanta Inhalation Rate. The quanta inhalation rate is computed as:

$$q_{\text{inhaled}} = q_{\text{concentration}} \times \text{Breathing Rate} \times \text{Duration} \times (1 - \text{Mask Inhalation Efficiency} \times P[\text{Wear Mask}])$$

Values for the Mask Inhalation Efficiency, as well as for the breathing rate (which varies by activity) can be found at the bottom of this page. For the sake of completeness and to make this manuscript self-contained, we have included the tables suggested by Jimenez [69] in Appendix E (Figures 12, 13, and 14), and refer to the sources he suggests for a more fine-grain estimate of what these should be⁶.



(a) Decay rate as a function of UV and relative humidity, for a temperature of 20° Celsius.

(b) Decay rate as a function of UV and temperature (in Celsius, for a relative humidity of 40%).

Figure 10: Decay rate of the virus, reproduced from [86, 87], and as a function of humidity, UV index, as well as temperature. NA values appear as transparent tiles.

Ventilation Rates. The ventilation rate per person is computed as:

$$\text{Ventilation} = \frac{1}{n_{\text{tot}}} \times \text{Volume} \times \text{Ventilation with outside air} \times \frac{1000}{3600}$$

where n_{tot} is the total number of participants, and the ventilation rate is measured in L^{-1}/s and depends on the activity. Again, for the sake of completeness, we have included in Appendix E (Figure 15) the table from the ASHRAE (American Society of Heating, Refrigerating and Air-Conditioning Engineers) listing all the activities as well as their corresponding ventilation rates⁷ that were suggested by Jimenez [69] to perform the computations.

⁶ Link to the EPA website: <https://www.epa.gov/expobox/exposure-factors-handbook-chapter-6>

⁷ Link to the ASHRAE tables: https://ashrae.iwrapp.com/ASHRAE_PREVIEW_ONLY_STANDARDS/STD_621_2019

Appendix C: Sensitivity Analysis

Whilst we have based our estimates of the different parameters used in this model on the literature, and tried to incorporate estimates of their uncertainty to try and correctly estimate our confidence in the output of the model, this is nevertheless contingent on several choices on (a) the probability that a ticket holder will lie and fail to report symptoms on the day of the event in order to get into the event, and (b) the efficiency of the masks, and input parameters in the room.

(a) Probability of lying. As explained in the introduction, the risk model that we aim to develop has to be context-aware. That is, the estimates of the risk that the model should output should depend (a) on the prevalence at the time of the event and (b) on the ticket holder's vaccination status. The only input that requires to be determined is the propensity of people to lie if they have symptoms. This is a priori a difficult parameter to estimate, which would be required to be informed by sociology studies. As the CAPACITY study proceeds, this is in particular one of the parameters that we hope to be able to inform better. However, in the absence of information as to what value of that parameter should be set, we propose here a sensitivity analysis to show that the model is in fact relatively weakly sensitive to the choice of this particular parameter. We show the different infectiousness curves corresponding to different values of the parameter p_{lie} in Fig. 8 and 9. As shown in Fig. 8, this probability of lying impacts the value of the maximum probability of infectiousness at the event: this value is maximal at 4 days before the event, with a value of 42.1% if the participants never lie, 48% if these participants lie half of the time, and 53% if they always lie. This represents a 25.8% increase in probability from a scenario where participants are considered as completely trustworthy to one where these participants are considered as unreliable. Table 4 quantifies the impact of this parameter in the case of the Royal Albert Hall in order to assess the sensitivity of the entire pipeline to this particular choice of parameter in two situations: low prevalence (August 3rd 2020) and high prevalence (January 18th 2021). As denoted in this table, the impact of this parameter is small in situations where the prevalence is already small. More substantial deviations occur when the prevalence increases, and such deviations are especially important in the tails (here, the median increases by 6 cases (35%) while the 97.5th prediction interval increased by 29% (69 cases) in situations of high prevalence between $p_{lie}=0$ and $p_{lie}=1$. While the relative increase (29%) is important, the absolute difference (69 cases) is small compared to the uncertainty in the prevalence (1245 (sd 375) cases).

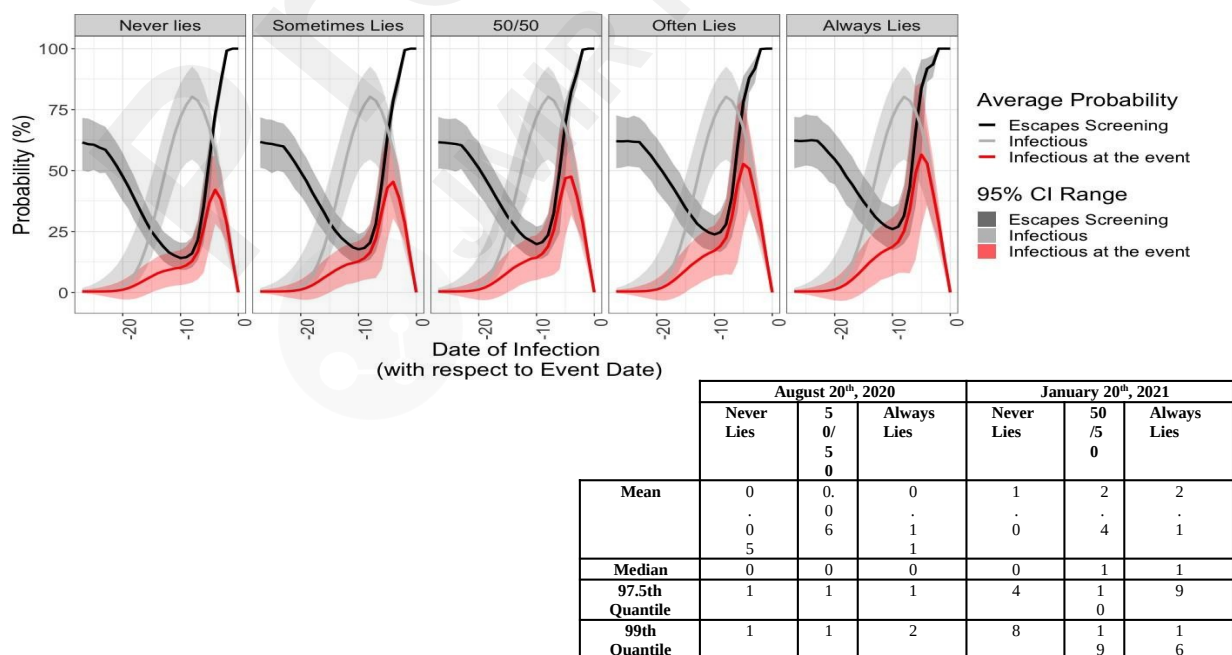


Figure 11: Analysis of the sensitivity of our infectiousness estimation to various values of the probability of lying

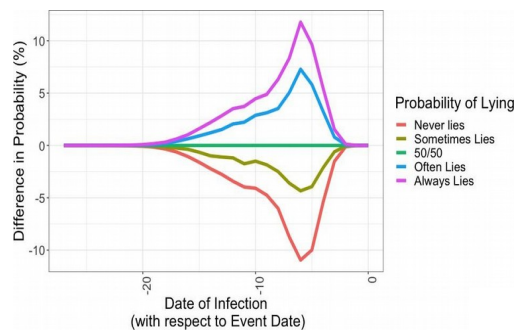


Figure 9: Analysis of the sensitivity of our infectiousness estimation to various values of the probability of lying.

Table 4: Quantitative comparison of the sensitivity of the results (number of transmissions at the event) as a function of p_{SC} . While the absolute difference between the scenarios remains reasonable for the mean, this difference becomes particularly important in the tails of the distribution (97.5th and 99th quantiles).

Mask Efficiency. Another parameter of great importance in the model consists of the effect of the mask efficiency. To this end, we contrast again a scenario with 100% of mandatory mask wearing, but with exhaled efficiency varying from 30, 50, 70, and 90% (the inhaled breathing being fixed efficiency to 50% – the same phenomenon would hold if varying the inhaled breathing efficiency). The results are presented in Table 5. We note the importance sensitivity of the results in the tails of the distribution: the absolute difference (in terms of number of cases) diverges significantly when looking at the 97.5th quantile of the distribution for instance. This highlights the efficiency of masks in limiting superspreading phenomena. We hope to use in particular the results of the CAPACITY study (and behavioural factors such as abidance to mask wearing, preferred type of mask, etc.) as well as the growing literature of mask efficiency to be able to refine our estimate of the mask efficiency. In the meantime, in this paper, we use the conservative 50% efficiency (lower bound provided in [67]).

Discussion. In the modelling, we neglect any correlation between ticket holders, however this is unlikely to hold in real life as some might come from the same household. Given participants from the same household would all be rejected if one of them were to test positive, this simplification is likely to be a conservative estimate. Due to the nature of the problem and gaps in what is known about transmission risks, our model does not contend to make precise estimates of the form “we expect x numbers of cases” as a result of the event. Rather, it should be taken as a means of providing a scale of the risk and is best used to make comparisons, for example against a null model in which the event does not occur but individuals still get infected in the community. As such, our methodology provides a relative quantification of that risk such as “holding the

| Mask Efficiency (%) | August 20 th , 2020 | | | | January 20 th , 2021 | | | |
|---------------------|--------------------------------|------|------|------|---------------------------------|-----|-----|-----|
| | 30 | 50 | 70 | 90 | 30 | 50 | 70 | 90 |
| Mean | 0.08 | 0.06 | 0.04 | 0.01 | 3.5 | 2.4 | 1.5 | 0.5 |
| Median | 0 | 0 | 0 | 0 | 2 | 1 | 1 | 0 |
| 97.5 Quantile | 1 | 1 | 0 | 0 | 14 | 10 | 6 | 3 |
| 99th Quantile | 2 | 1 | 1 | 0 | 27 | 19 | 11 | 5 |

Table 5: Sensitivity of the results to mask efficiency. Note the significant absolute difference in the tails of the distribution.

event is expected to increase the number of cases by x% in this pool of participants.” The use of Monte Carlo simulations allows us to account for some uncertainty in our model, and to produce more meaningful risk estimates. As our second goal is to quantify the efficiency of the screening protocol, this pipeline can be run using different screening protocols or testing strategies to determine their efficiency. We also hope to be able to further develop this pipeline through (a) leveraging in-situ data collection and (b) refinement of the models themselves. In particular, using a fully anonymous, post-event questionnaire, we would evaluate participants’ compliance with the screening protocol, as well as with the safety measures at the time of the event. As more events are held, we can quantify the success of our pipeline to provide coverage of the observed number of infections. From the model perspective, we hope to explore further extensions to the current aerosol transmission model, which is based on the Wells-Riley model and so assumes uniform mixing of the quanta in the venue. Using information on the potential induced cases (e.g., their relative seating distance), we aim to refine this model by studying ways of accounting for the spatial heterogeneity of the quanta distribution.

Appendix D: Risk Communication

Vaccine passports and widespread antigen tests – a false sense of security? The use of vaccine passports for international air travel has ignited significant debate in the UK and even more controversial is their use for entry to mass, live events [12]. Notwithstanding the challenges surrounding operational verification of vaccine certification, the ethical implications of excluding those unable or unwilling to be vaccinated from participating in normal social encounters and the resulting implications for social inequities [13], the use of vaccine certification to permit entry to an event will likely significantly overestimate its safety. Vaccinated individuals may still be infected with SARS-CoV-2. Even antigen-test based screenings of ticket holders prior to an event will likely overestimate the safety of the event as some tests will be falsely negative. The definition of what constitutes an admissible level of risk thus poses a difficult conundrum to the live event industry.

CAPACITY-UK. The motivating application behind this paper is the CAPACITY study [32]— a partnership between CERTIFIC (a private, remote testing, health status and identify certification service) and Imperial College London – to predict and measure the outcomes of full capacity live events whilst ensuring rigorous abidance by public health and safety measures. Central to this study is the efficiency of pre-event screening by testing all ticket holders using professionally-witnessed rapid at-home antigen tests, and post-event monitoring based on antigen tests, surveys, and safety recommendations. Mass rollout of home-based Lateral Flow Testing to all adults in the UK [88] for twice weekly testing ensures that all households will already have the tests available to them. CAPACITY-UK proposes simply for the tests to be professionally witnessed via the CERTIFIC application to overcome the trust issue, verifying that tests have been collected and conducted to the appropriate standard. In addition to testing (which is susceptible to false positives and negatives), the CAPACITY protocol gathers anonymized information on participant vaccination status, regional address, and a few basic questions regarding individual characteristics (see Fig. 10). The purpose of this additional information is to allow the design of a tailored risk estimation model — both at the participant and at the community level. Such risk estimates are central to the protocol: not only are they necessary in the context of informed consent and communicating to the ticket holders their own level of risk so that they may choose to attend the event, but they are also essential in informing event managers and policy makers on the likelihood of an outbreak. This system potentially allows for the management of full capacity, live events – a crucial parameter for commercial viability of the industry. Moreover, contrary to the issues surrounding vaccination passports, vaccination status would be requested, but not required for attendance – particularly if overall risk of transmission at the event remains within acceptable bounds.

This system potentially allows for the management of full capacity, live events – a crucial parameter for commercial viability of the industry. Moreover, contrary to the issues surrounding vaccination passports, vaccination status would be requested, but not required for attendance – particularly if overall risk of transmission at the event remains within acceptable bounds.

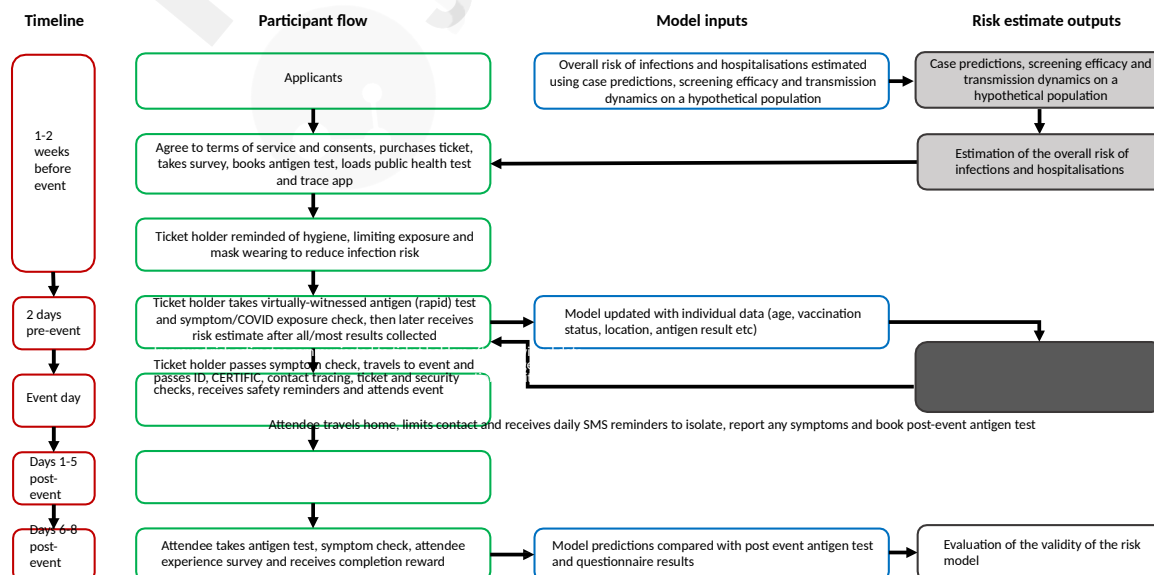


Figure 10: CAPACITY process flow from the ticket holder perspective. On the left-hand side in red lined boxes are the timings of various stages in CAPACITY process flow. In the middle the process flow is described from the participant perspective. On the right-hand side, the interaction between user-supplied data and model-generated risk estimates is described. The certainty in the model output is conveyed through the varying shades of grey (the darker the colour, the more certain the model).

Risk Communication. The risk estimate is then provided to the participants using a variety of different formats, for better interpretability and communicability of the risk to the general public. Fig 11 shows a few examples of the displays used by the CAPACITY study.

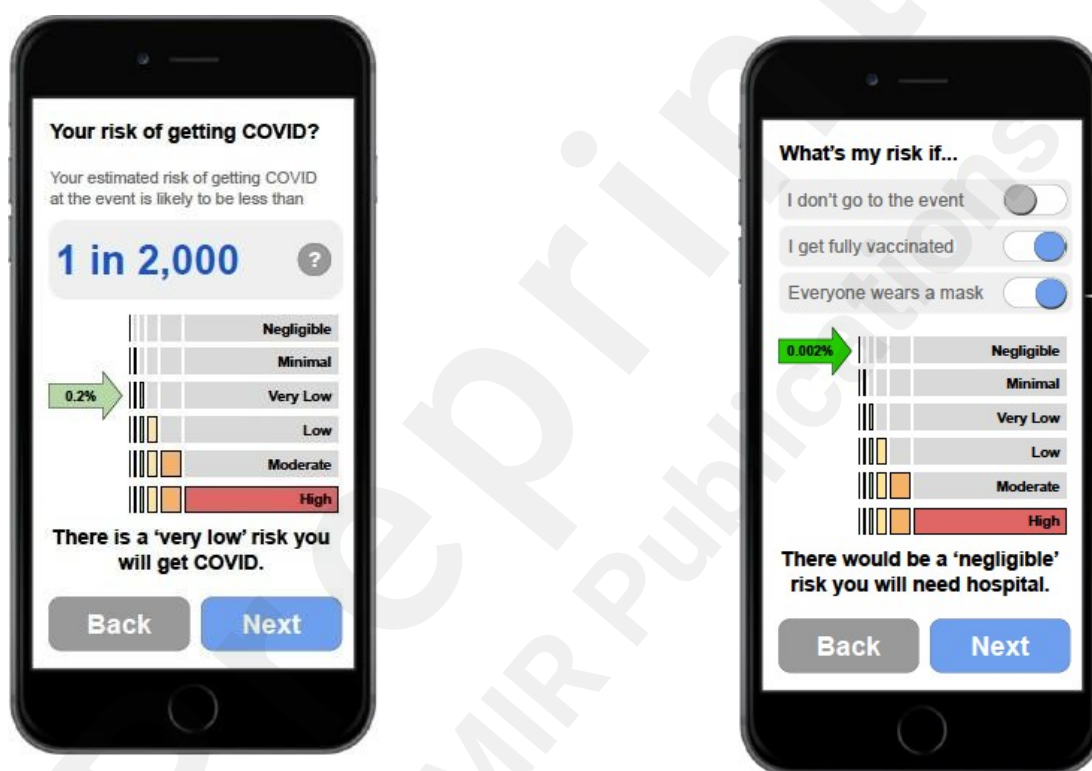


Figure 11: Top left – baseline estimates; Top right – final estimates; Bottom left – individual risk communication; Bottom right – tailored risk scores under different scenarios

Dashboard. The dashboard for event organizers is an R Shiny app that asks organizers to input relevant information on the event and generates predictions of the number of new infections that emerge from transmission during the event. The dashboard is divided into two main sections: 'What are the parameters for the event?' and 'What are the results?'. The first section includes input fields for the event location, duration, and participant information. The second section displays the results of the simulation, including the number of new infections, the number of people who become ill, and the number of people who require hospitalization. The results are presented in a clear and concise manner, using charts and tables to visualize the data. The dashboard is designed to be user-friendly and easy to navigate, allowing organizers to quickly understand the potential impact of their event and make informed decisions about how to manage it.

Which country will the event be in
United Kingdom

Total number of people present at the event
1000

When will the event occur?
2021-08-28

Duration of the event (in minutes)
90

Probability of lying: pretending to feel fine even with symptoms
0.5

What proportion (%) of the participants do you expect to wear any mask?
50

Figure 12: Input fields in the event planning dashboard

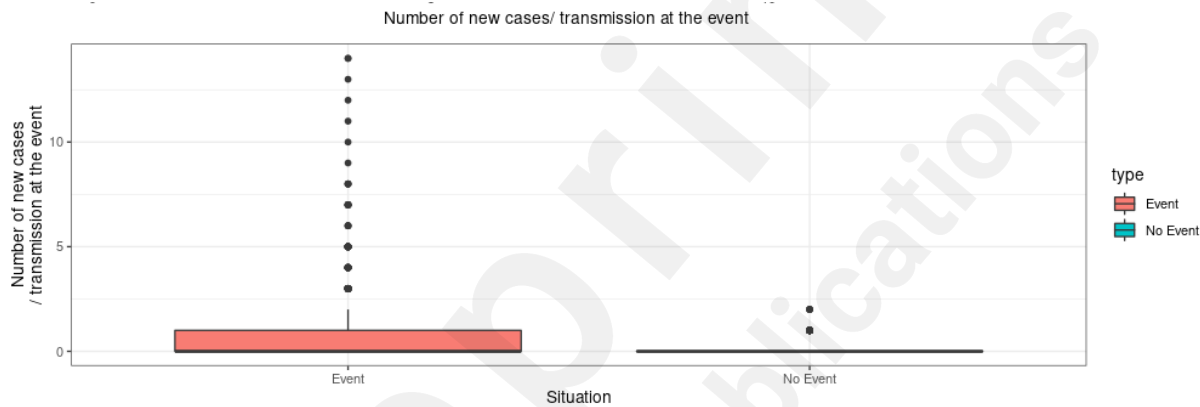


Figure 13: Sample simulation results for new infections during the event

Appendix E: Model Validation

Model Validation is a crucial step in allowing this model to be deployed and trusted. In the previous appendices, we have run experiments on the prevalence estimation and vaccination status – allowing us to highlight and quantify the performance and reliability of these steps – but not on the transmission setting, due to the scarcity of available data. The transmission dynamics in our model are based on the Jimenez aerosol transmission model, which was retro-actively fitted from documented transmission events. This transmission step is in fact the most difficult one to validate: there are none or very few available datasets on COVID spread either following live events or tracking super spreader events, nor are there any statistics on how likely super spreader events are. As such, the majority of super spreader events that are documented currently (a) are generally not detailed enough to untangle the huge variability in context (outdoors vs indoors, activity performed, background prevalence, etc), and (b) suffer from selection bias --- and might not be reflective of the general distribution of events.

However, to overcome this hurdle and to try and make use of the currently available data, we propose the three following directions:

- a. **Comparison with existing Super Spreader Event databases.** We begin our validation of the aerosol transmission model by using an openly available dataset with documented accounts of super spreader events [91]. This dataset is an open-source, manually curated database with now more than 1,600 Super-Spreading Events (SSEs) from around the world. These superspreading events are varied both in length (short events such as parties, extended co-living such as in dorms, prisons, or nursing homes), nature (sport participation, bar crawl, restaurant), or context (indoors, outdoor) to name a few. Despite the potential heterogeneity of this dataset and the selection bias that these events are likely to suffer from, we propose using this dataset as a way of validating the behaviour of our estimates, and their ability to model super spreader events. We begin by investigating the behaviour of the proportion of people infected at these events. To this end, we consider the events for which the number of participants and the total number of cases (before and after the event) are available. The following figure shows a plot of the percentage of people infected as a function of the event size. The blue line is the fitted loess line, along with its associated confidence interval. We note the strong spread of the percentage of people infected --- going anywhere from a few to 100% and yielding the following conclusion:
Lesson 1: In superspreader events (SSEs), the number of people infected is highly volatile. In particular, for small events, 100% secondary infections is not an unlikely scenario. The percentage of the crowd infected decreased however the size of the crowd.

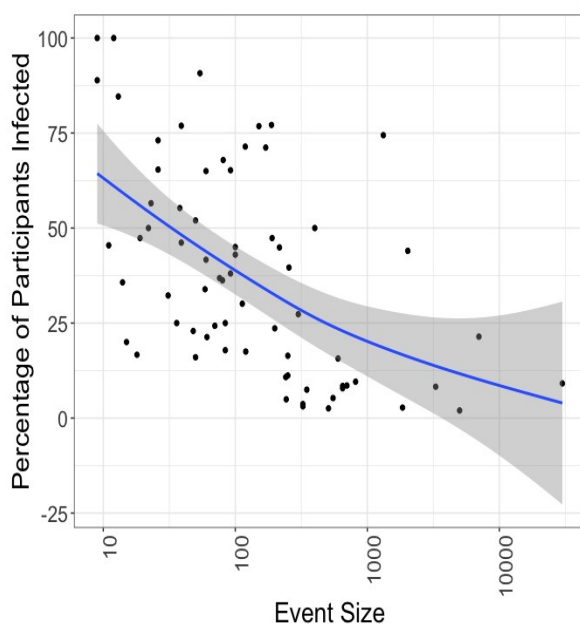


Figure E1: Percentage of Participants infected as a function of the event size. The blue line is the fitted loess function, with associated confidence interval.

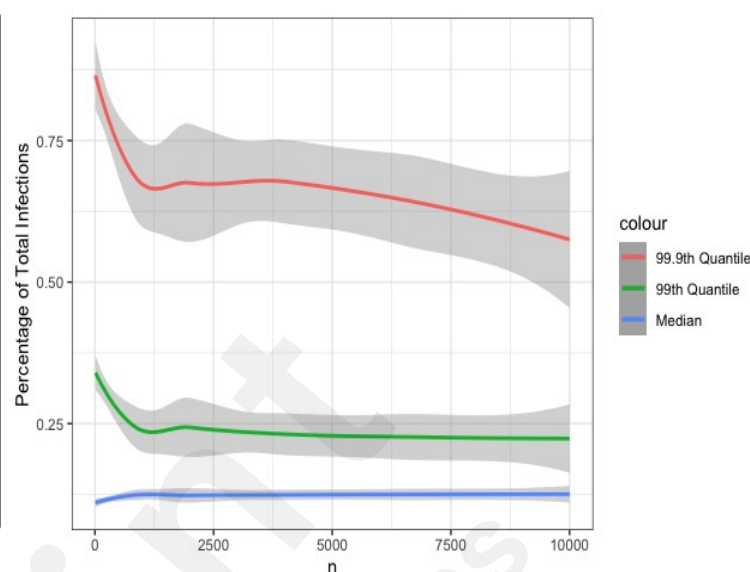


Figure E2 Simulation on the percentage of secondary cases according to our model .

Model sanity check n°1: We check if our current model behaves the same. Considering a scenario where 10% of the participants are initially infected, we vary the number of people at the event (whilst keeping the same density as our event in the RAH --- which we believe to be a reasonable approximation: larger events are not necessarily more dense than small gatherings), and check that we do observe a decreasing relationship between event size and proportion of secondary cases. The following figure highlights the result of 10,000 simulations per event size. It is reassuring to see that the upper quantiles (ie, the 99.9th quantiles) of these distributions (which correspond to potential super spreader events) follow the same decreasing behaviour as observed in the SSE dataset.

Model sanity check n°2: As a way of further assessing the validity of our model, we further filter the dataset for the recorded events for which the number of Index cases and the total number of secondary cases is available: this allows us to look at the transmissions at the event itself, this disentangling high transmissions due to high prevalence or high number of index cases. This results in a dataset of 26 indoor events. To limit the heterogeneity of the dataset, we stratify the events into two categories: “close” transmission settings (where the participants are expected to be in close proximity to one another, or a density less than 1 participant per square meter. This is meant to mimic scenarios such flights, or meal sharing), and “medium” (where the participants are farther apart --- such as in an office, or a density more than 1 participant per 9 square meter). These rates are displayed in Figure 3 (blue line denotes the fitted loess, along with confidence interval). We note again the high spread of the number of secondary cases--- indicating the high stochasticity of superspreading. We then proceed to assess whether our model would be able to account for these events. Using the ventilation parameters from the RAH example (which we think to be standard) and the two aforementioned densities, we simulate events of 90 minutes with the same number of participants and index cases. The purpose of this experiment is to check if the number of infections is achievable by the model. Note that this is again a sanity check, rather than a real statistical test. The super spreader events in this dataset are far too heterogeneous (in density, length. etc). Stratifying events according to close/medium proximity attempts to limit some of this heterogeneity.

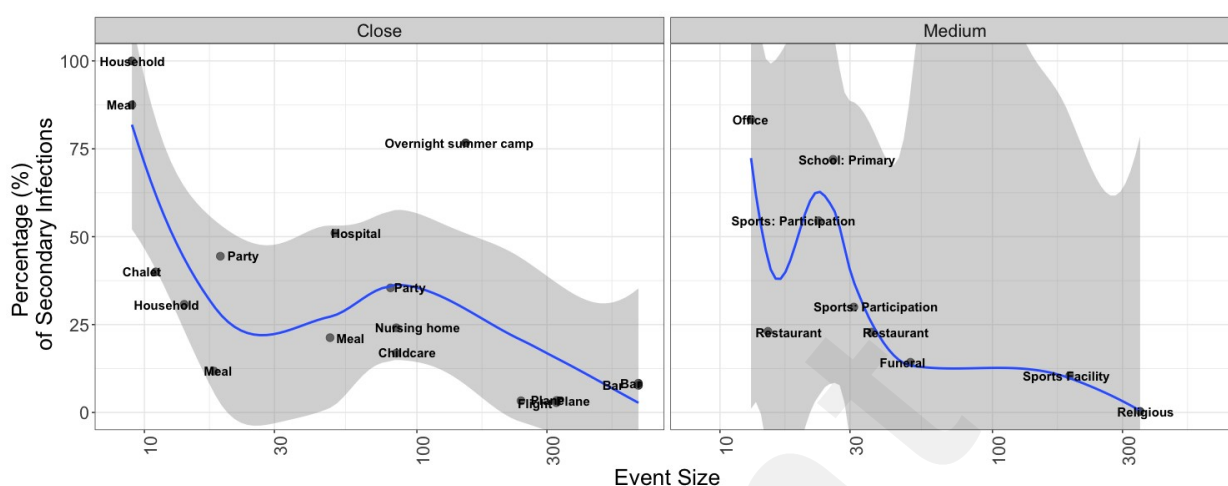


Figure 3: Proportion of Secondary Cases as a function of event size, stratified by proximity of the participants.

Using 10,000 simulations, we obtain the distributions highlighted in Figure 4. Most of these events are indeed qualified as superspreaders by our model--- which is reassuring. This does allow us to conclude that the numbers offered by our model are not unreasonable: most of the events in this dataset are indeed outliers according to our model, but they also fall within the realm of the model's outputs.

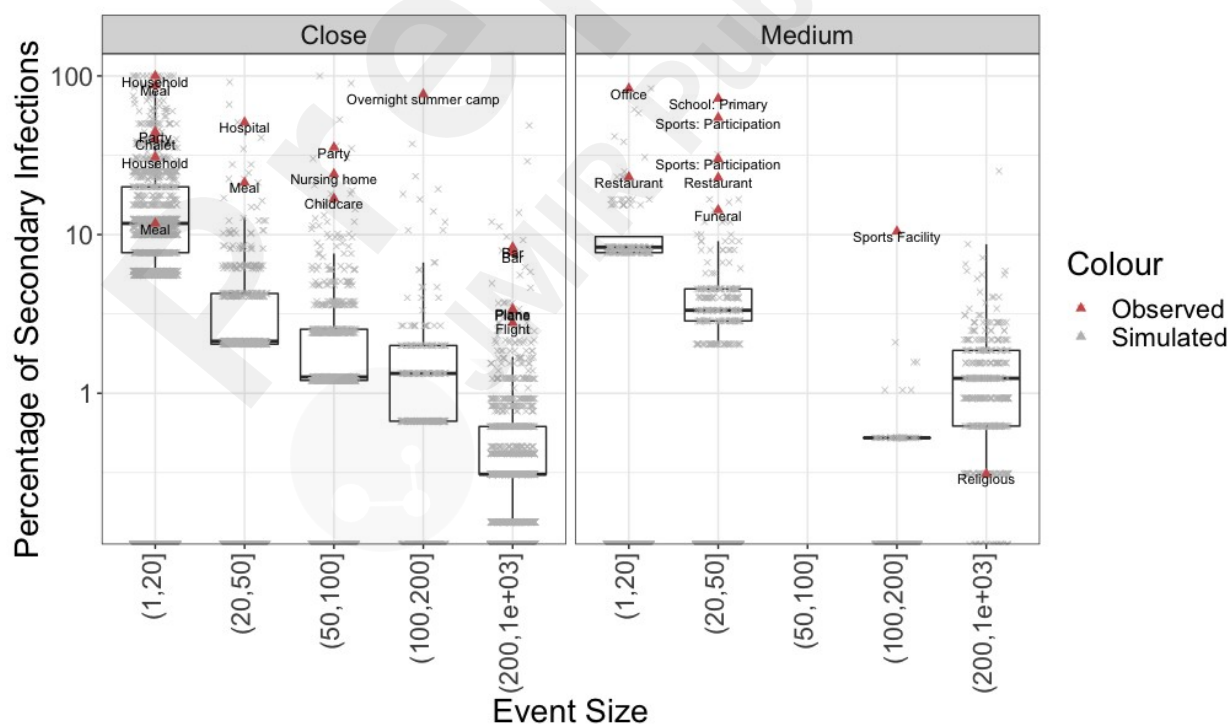


Figure 4: Observed vs simulated percentage of secondary infections occurring at potential super spreader events. The figure is faceted into two categories of events where the likely distance between people is ~1m (Close) or >1m (Medium). Events are further grouped on the x axis by the number of attendees. The percentage of people infected at the event (secondary infections) is indicated on the y axis with grey crosses indicating simulation results, and red triangles indicating observed cases.

- b. **Benchmarking using the first live event studies:** In terms of randomised controlled trials or planned observational studies, we are aware of only of three that have been performed with sufficient information to validate or inform our model:

1. ***The Barcelona Winter concert:*** Revollo et al., [89] reported that in a randomised controlled trial for a live indoor music event held in Barcelona on December 12th, 2020, 0 out of 465 in the experiment (live-event) arm were Ag-RDT positive, and 2 out of 495 in the control (no-event arm). Their screening process is roughly similar to the one used by CERTIFIC. We use this documented event to benchmark our model as follows:

- a) *Prediction scenario:* assuming that we wanted to predict all transmissions for such an event 4 weeks in advance. We run our prediction scenario for this indoor event, using the parameters described by the authors. According to these simulations, around 9.2 participants should have been infected, with an average of 0.56 infected participants passing through the screening process and entering the event. The number of predicted transmissions was 0.21 (CI: 0-2), which is in line with what was observed at the event.
- b) *Transmission validation:* We now replace the prevalence imputation part by the observed data, and focus on analyzing the transmission outcomes. On average, 5.89 should have been infected prior to the event, of which 4.98 should have been detected. The observed number of detections (0) among participants are lower than expected: the probability that no participant is detected as positive is 0.022 according to our model. This could be due to response/selection bias in the study cohort. This also indicates that our estimates (which assume the public to be sampled from the general Spanish public) will be conservative. Despite being conservative, the lack of transmission falls again within what is predicted by our pipeline – thereby validating our model outputs.

2. ***The Barcelona Spring concert:*** Llibre et al., [90] observed 6 out of 5,000 Ag-RDT positives before a live music event held in Barcelona on March 27th, 2021 and 6 out of 4584 within 2 weeks after the event. Their screening process is roughly similar to the one used by CERTIFIC. We run our model as a benchmark. Using the observed incidence, we predict that an average of 8.47 should have been detected as positive by the screening process --- so that detecting exactly 6 individuals (as occurred in this event) has probability 0.1 and falls within the realm of likely observations. Moreover, this study shows that a total of 6 participants tested positive for COVID within 2 weeks of the event: 3 of which were likely to have been contaminated through other index cases, and one woman who was likely to have been in her incubation phase during the concert. The transmission source for the remaining two was not identified, and could stem from outside contamination or transmission at the concert. As such, supposing that the worst case total number of infectious participants at the event was likely to be 4 participants or more (probability of 0.04 in our model), the probability that it would result in 2 infections or less is 0.98 in our model. As such, this event falls within the realms of likely possibilities according to our model – thereby providing further reassurance as to the validity of the model.

3. ***Prospective data: The CAPACITY Study, with one event to date: Standon Calling.*** In a recent collaboration between Imperial College London, CERTIFIC and the Standon Calling family music festival (22-25 July 2021) an at-home, video-testing certification process was piloted resulting in clinically-certifiable LFT test results from CERTIFIC- a provider of services in line with standards overseen by a UK Government authorised private testing provider. 15,612 tickets were sold, and the festival had a total duration of four days. 40 participants tested positive upon entry, 10 of which were likely false positives. Data is currently being collected, and post-participation surveys sent out to assess the magnitude of

transmission events. We plan on using this event as well as subsequent events ran by CERTIFIC as a way of further validating the model.

Note that these are only a few (two) realizations of an inherently volatile, stochastic process — with high heterogeneity in conditions (outdoors, indoors, etc). The power of this analysis can only be very limited: currently, this simply serves as another reassurance/“sanity check” that our model manages to produce estimates that are likely, rather than as an actual statistical validation step. However, as the number of live events increase, we hope to be able to add more data to corroborate the validation of our pipeline.

c. Active Data Collection. The lack of data is currently a real issue, that can only be overcome by starting a rigorous data collection process – one that is amenable to help calibrating the transmission process, and that must include information about the event (number of people, density, etc). To this end, we have added a questionnaire that people can fill in on our R-Shiny app [94], and that would help us expand the number of gathering/ live events. We are hoping that event organizers and individuals (involved in planning ceremonies, weddings, any type of gatherings) could look at our risk estimates, and volunteer to submit their data – thereby allowing a more scalable data collection process. In fact, one of our objectives in publishing our model and making it easy to access is to encourage the data collection that is so desperately needed for risk assessment, validating risk calculators and improving current transmission models.

Appendix F: Reference Tables

| Table 6-1. Recommended Long-Term Exposure Values for Inhalation (males and females combined) | | | | | |
|---|----------------------------|------------------------|--|---|---|
| Age Group ^a | Mean (m ³ /day) | Sources Used for Means | 95 th Percentile ^b (m ³ /day) | Sources Used for 95 th Percentiles | Multiple Percentiles |
| Birth to <1 month | 3.6 | c | 7.1 | c | |
| 1 to <3 months | 3.5 | c, d | 5.8 | c, d | |
| 3 to <6 months | 4.1 | c, d | 6.1 | c, d | |
| 6 to <12 months | 5.4 | c, d | 8.0 | c, d | |
| Birth to <1 year | 5.4 | c, d, e, f | 9.2 | c, d, e | |
| 1 to <2 years | 8.0 | c, d, e, f | 12.8 | c, d, e | |
| 2 to <3 years | 8.9 | c, d, e, f | 13.7 | c, d, e | |
| 3 to <6 years | 10.1 | c, d, e, f | 13.8 | c, d, e | See Table 6-4, Table 6-6 through Table 6-8, Table 6-10, Table 6-14 Table 6-15 [none available for Stifelman (2007)] |
| 6 to <11 years | 12.0 | c, d, e, f | 16.6 | c, d, e | |
| 11 to <16 years | 15.2 | c, d, e, f | 21.9 | c, d, e | |
| 16 to <21 years | 16.3 | c, d, e, f | 24.6 | c, d, e | |
| 21 to <31 years | 15.7 | d, e, f | 21.3 | d, e | |
| 31 to <41 years | 16.0 | d, e, f | 21.4 | d, e | |
| 41 to <51 years | 16.0 | d, e, f | 21.2 | d, e | |
| 51 to <61 years | 15.7 | d, e, f | 21.3 | d, e | |
| 61 to <71 years | 14.2 | d, e, f | 18.1 | d, e | |
| 71 to <81 years | 12.9 | d, e | 16.6 | d, e | |
| ≥81 years | 12.2 | d, e | 15.7 | d, e | |
| ^a When age groupings in the original reference did not match the U.S. EPA groupings used for this handbook, means from all age groupings in the original reference that overlapped U.S. EPA's age groupings by more than one year were averaged, weighted by the number of observations contributed from each age group. Similar calculations were performed for the 95 th percentiles. See Table 6-25 for concordance with U.S. EPA age groupings. ^b Some 95 th percentile values may be unrealistically high and not representative of the average person. ^c Arcus-Arth and Blaisdell (2007). ^d Brochu et al. (2006b). ^e U.S. EPA (2009a). ^f Stifelman (2007). | | | | | |

Figure 12: Inhalation rates. Link to the EPA website: <https://www.epa.gov/expobox/exposure-factors-handbook-chapter-6>

| Table 6-2. Recommended Short-Term Exposure Values for Inhalation (males and females combined) (continued) | | | | |
|--|---------------------|----------------------------------|---|----------------------|
| Activity Level | Age Group (year) | Mean (m ³ /minute) | 95 th Percentile (m ³ /minute) | Multiple Percentiles |
| Light Intensity (continued) | 21 to <31 | 1.2E-02 | 1.6E-02 | |
| | 31 to <41 | 1.2E-02 | 1.6E-02 | |
| | 41 to <51 | 1.3E-02 | 1.6E-02 | |
| | 51 to <61 | 1.3E-02 | 1.7E-02 | |
| | 61 to <71 | 1.2E-02 | 1.6E-02 | |
| | 71 to <81 | 1.2E-02 | 1.5E-02 | |
| | ≥81 | 1.2E-02 | 1.5E-02 | |
| Moderate Intensity | Birth to <1 | 1.4E-02 | 2.2E-02 | |
| | 1 to <2 | 2.1E-02 | 2.9E-02 | |
| | 2 to <3 | 2.1E-02 | 2.9E-02 | |
| | 3 to <6 | 2.1E-02 | 2.7E-02 | |
| | 6 to <11 | 2.2E-02 | 2.9E-02 | |
| | 11 to <16 | 2.5E-02 | 3.4E-02 | |
| | 16 to <21 | 2.6E-02 | 3.7E-02 | |
| | 21 to <31 | 2.6E-02 | 3.8E-02 | |
| | 31 to <41 | 2.7E-02 | 3.7E-02 | |
| | 41 to <51 | 2.8E-02 | 3.9E-02 | |
| | 51 to <61 | 2.9E-02 | 4.0E-02 | |
| | 61 to <71 | 2.6E-02 | 3.4E-02 | |
| | 71 to <81 | 2.5E-02 | 3.2E-02 | |
| | ≥81 | 2.5E-02 | 3.1E-02 | |
| | | | | |
| High Intensity | Birth to <1 | 2.6E-02 | 4.1E-02 | |
| | 1 to <2 | 3.8E-02 | 5.2E-02 | |
| | 2 to <3 | 3.9E-02 | 5.3E-02 | |
| | 3 to <6 | 3.7E-02 | 4.8E-02 | |
| | 6 to <11 | 4.2E-02 | 5.9E-02 | |
| | 11 to <16 | 4.9E-02 | 7.0E-02 | |
| | 16 to <21 | 4.9E-02 | 7.3E-02 | |
| | 21 to <31 | 5.0E-02 | 7.6E-02 | |
| | 31 to <41 | 4.9E-02 | 7.2E-02 | |
| | 41 to <51 | 5.2E-02 | 7.6E-02 | |
| | 51 to <61 | 5.3E-02 | 7.8E-02 | |
| | 61 to <71 | 4.7E-02 | 6.6E-02 | |
| | 71 to <81 | 4.7E-02 | 6.5E-02 | |
| | ≥81 | 4.8E-02 | 6.8E-02 | |

Figure 13: Inhalation rates. Link to the EPA website: <https://www.epa.gov/expobox/exposure-factors-handbook-chapter-6>

| Table 6-2. Recommended Short-Term Exposure Values for Inhalation (males and females combined) | | | | |
|---|-------------------|-------------------------------|--|-------------------------------|
| Activity Level | Age Group (years) | Mean (m ³ /minute) | 95 th Percentile (m ³ /minute) | Multiple Percentiles |
| Sleep or Nap | Birth to <1 | 3.0E-03 | 4.6E-03 | See Table 6-17 and Table 6-19 |
| | 1 to <2 | 4.5E-03 | 6.4E-03 | |
| | 2 to <3 | 4.6E-03 | 6.4E-03 | |
| | 3 to <6 | 4.3E-03 | 5.8E-03 | |
| | 6 to <11 | 4.5E-03 | 6.3E-03 | |
| | 11 to <16 | 5.0E-03 | 7.4E-03 | |
| | 16 to <21 | 4.9E-03 | 7.1E-03 | |
| | 21 to <31 | 4.3E-03 | 6.5E-03 | |
| | 31 to <41 | 4.6E-03 | 6.6E-03 | |
| | 41 to <51 | 5.0E-03 | 7.1E-03 | |
| | 51 to <61 | 5.2E-03 | 7.5E-03 | |
| | 61 to <71 | 5.2E-03 | 7.2E-03 | |
| | 71 to <81 | 5.3E-03 | 7.2E-03 | |
| Sedentary/ Passive | ≥81 | 5.2E-03 | 7.0E-03 | |
| | Birth to <1 | 3.1E-03 | 4.7E-03 | |
| | 1 to <2 | 4.7E-03 | 6.5E-03 | |
| | 2 to <3 | 4.8E-03 | 6.5E-03 | |
| | 3 to <6 | 4.5E-03 | 5.8E-03 | |
| | 6 to <11 | 4.8E-03 | 6.4E-03 | |
| | 11 to <16 | 5.4E-03 | 7.5E-03 | |
| | 16 to <21 | 5.3E-03 | 7.2E-03 | |
| | 21 to <31 | 4.2E-03 | 6.5E-03 | |
| | 31 to <41 | 4.3E-03 | 6.6E-03 | |
| | 41 to <51 | 4.8E-03 | 7.0E-03 | |
| | 51 to <61 | 5.0E-03 | 7.3E-03 | |
| | 61 to <71 | 4.9E-03 | 7.3E-03 | |
| | 71 to <81 | 5.0E-03 | 7.2E-03 | |
| Light Intensity | ≥81 | 4.9E-03 | 7.0E-03 | |
| | Birth to <1 | 7.6E-03 | 1.1E-02 | |
| | 1 to <2 | 1.2E-02 | 1.6E-02 | |
| | 2 to <3 | 1.2E-02 | 1.6E-02 | |
| | 3 to <6 | 1.1E-02 | 1.4E-02 | |
| | 6 to <11 | 1.1E-02 | 1.5E-02 | |
| | 11 to <16 | 1.3E-02 | 1.7E-02 | |
| | 16 to <21 | 1.2E-02 | 1.6E-02 | |

Figure 14: Inhalation rates. Link to the EPA website: <https://www.epa.gov/expobox/exposure-factors-handbook-chapter-6>

TABLE 6.2.2.1 Minimum Ventilation Rates in Breathing Zone
(Table 6.2.2.1 shall be used in conjunction with the accompanying notes.)

| Occupancy Category | People Outdoor Air Rate R_p | | Area Outdoor Air Rate R_a | | Notes | Default Values | | | |
|---------------------------------|-------------------------------------|----------------|-----------------------------------|--------------------|-------|---|---|----------------|--------------|
| | cfm/ person | L/s· person | cfm/ft ² | L/s·m ² | | Occupant Density (see Note 4) | Combined Outdoor Air Rate (see Note 5) | | |
| | | | | | | #/1000 ft ² or #/100 m ² | cfm/ person | L/s· person | Air Class |
| Correctional Facilities | | | | | | | | | |
| Cell | 5 | 2.5 | 0.12 | 0.6 | | 25 | 10 | 4.9 | 2 |
| Dayroom | 5 | 2.5 | 0.06 | 0.3 | | 30 | 7 | 3.5 | 1 |
| Guard stations | 5 | 2.5 | 0.06 | 0.3 | | 15 | 9 | 4.5 | 1 |
| Booking/waiting | 7.5 | 3.8 | 0.06 | 0.3 | | 50 | 9 | 4.4 | 2 |
| Educational Facilities | | | | | | | | | |
| Daycare (through age 4) | 10 | 5 | 0.18 | 0.9 | | 25 | 17 | 8.6 | 2 |
| Daycare sickroom | 10 | 5 | 0.18 | 0.9 | | 25 | 17 | 8.6 | 3 |
| Classrooms (ages 5–8) | 10 | 5 | 0.12 | 0.6 | | 25 | 15 | 7.4 | 1 |
| Classrooms (age 9 plus) | 10 | 5 | 0.12 | 0.6 | | 35 | 13 | 6.7 | 1 |
| Lecture classroom | 7.5 | 3.8 | 0.06 | 0.3 | H | 65 | 8 | 4.3 | 1 |
| Lecture hall (fixed seats) | 7.5 | 3.8 | 0.06 | 0.3 | H | 150 | 8 | 4.0 | 1 |
| Art classroom | 10 | 5 | 0.18 | 0.9 | | 20 | 19 | 9.5 | 2 |
| Science laboratories | 10 | 5 | 0.18 | 0.9 | | 25 | 17 | 8.6 | 2 |
| University/college laboratories | 10 | 5 | 0.18 | 0.9 | | 25 | 17 | 8.6 | 2 |
| Wood/metal shop | 10 | 5 | 0.18 | 0.9 | | 20 | 19 | 9.5 | 2 |
| Computer lab | 10 | 5 | 0.12 | 0.6 | | 25 | 15 | 7.4 | 1 |
| Media center | 10 | 5 | 0.12 | 0.6 | A | 25 | 15 | 7.4 | 1 |
| Music/theater/dance | 10 | 5 | 0.06 | 0.3 | H | 35 | 12 | 5.9 | 1 |
| Multiuse assembly | 7.5 | 3.8 | 0.06 | 0.3 | H | 100 | 8 | 4.1 | 1 |

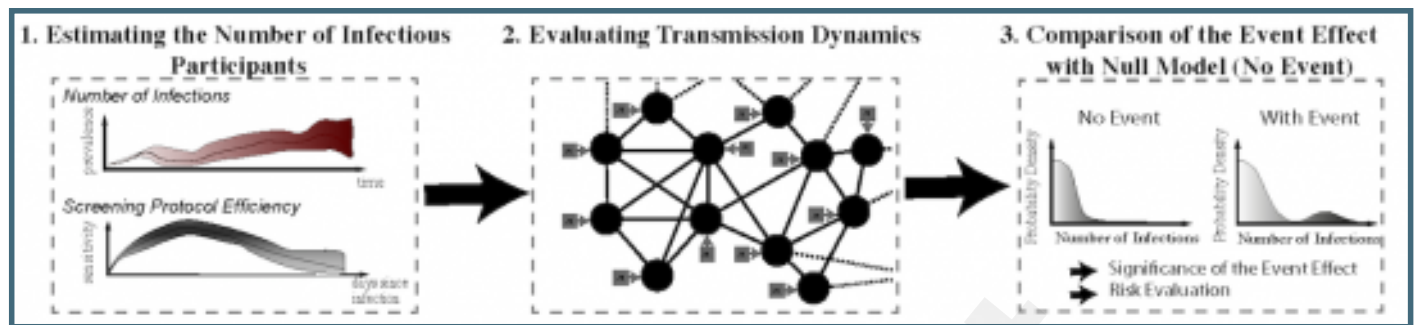
Figure 15: Ventilation Rates taken from the ASHRAE standards ⁸



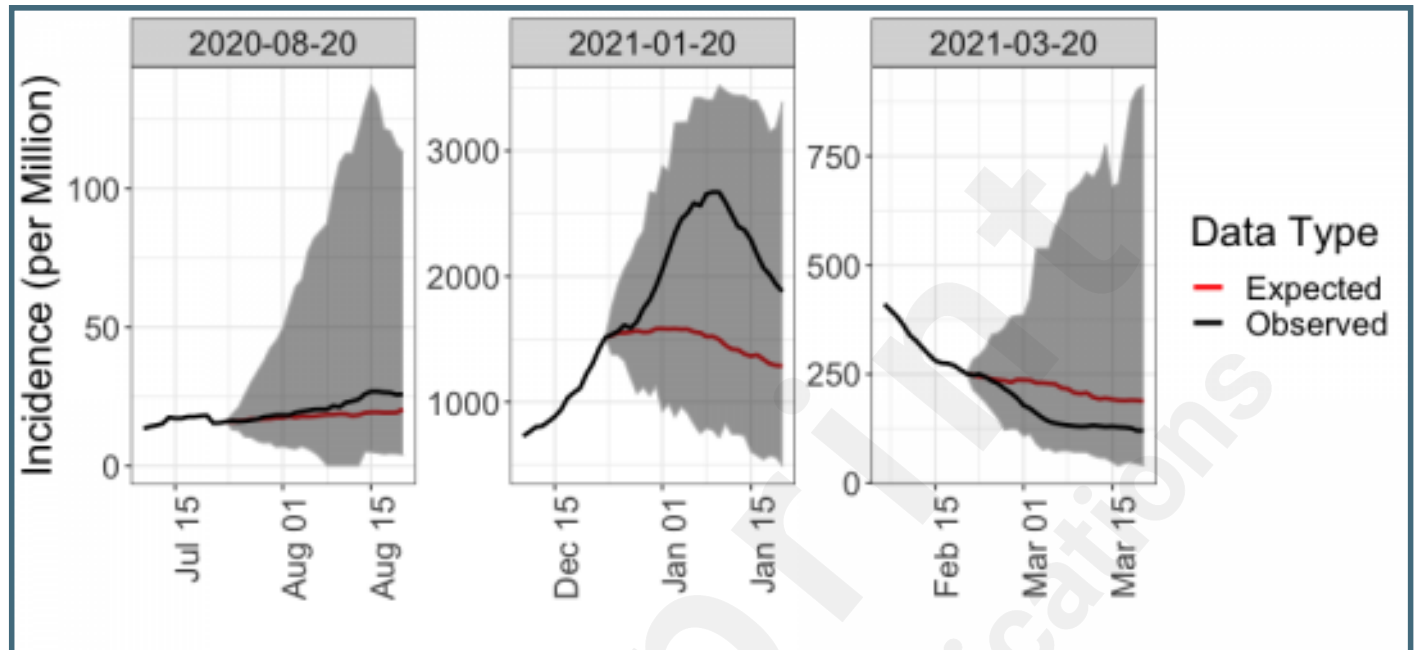
Supplementary Files

Figures

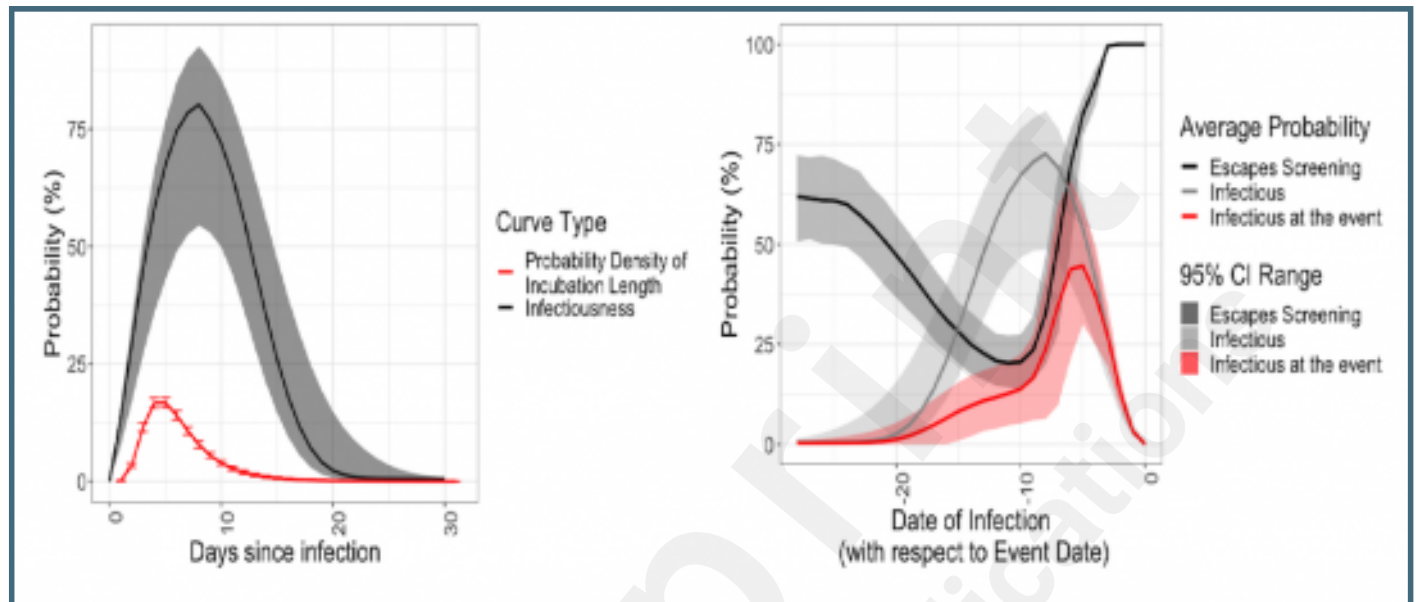
Summary of our modelling pipeline.



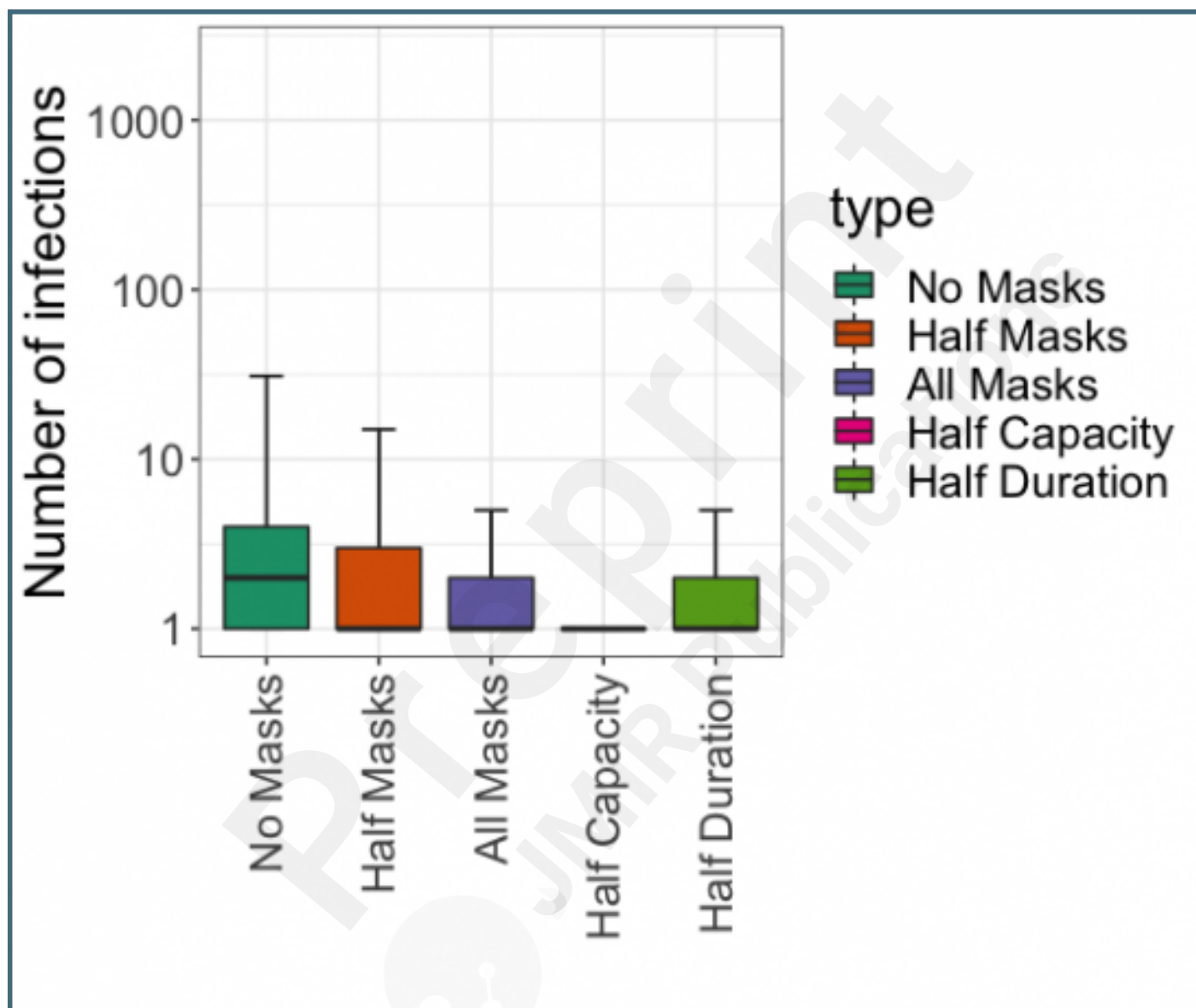
Projected incidence (average and 95% prediction interval) using a 100-nearest neighbour approach. The black line denotes observed incidence rates, while the red denotes the predicted ones (based on initial period of observation of $d=14$ days). The prediction interval for the predicted incidence over the next four weeks is highlighted in dark grey. We note that our k-NN method provides good coverage (the observed trajectory lies within the 95% prediction interval).



(a) Density of the COVID-19 incubation time, and Percentage culture positive. (b) Probability that an individual is infectious (light grey), that the screening protocol will miss them (black), and that they will be missed and so attend the event (red), as a function of days since infection. The shaded regions denote the uncertainty of this estimate due to the uncertainty on the sensitivity of the test. The distribution of the incubation time already integrates the uncertainty on the parameters μ and σ of the log-normal distribution.



Boxplots showing the distribution of the number of infections across different scenarios, for our RAH event held on March 20th 2021. Where variables are not mentioned, the number of attendees is 5,000, the duration is 3 hours, and the proportion of attendees wearing masks is 100%. Note that the distributional nature of these results is essential in highlighting nuances between scenarios: while holding an event at half capacity, or for half the duration produces average transmission risk that are roughly similar, holding the event at half capacity seems to more substantially reduce the effect of the event in the tails of the distribution.



Multimedia Appendixes

References and Appendices.

URL: <http://asset.jmir.pub/assets/360297abf63fe5d8238e1302254a0c2f.docx>

